Abstract

Interest in applying radar remote sensing for the study of forested areas led to the development of a model for scattering from corrugated stratified dielectric cylinders. The model is employed to investigate the effect of bark and its roughness on scattering from tree trunks and branches. The outer layer of the cylinder (bark) is assumed to be a low-loss dielectric material and to have a regular (periodic) corrugation pattern. It is further assumed that the corrugation exists in only the angular direction (two-dimensional problem). The inner layers are treated as lossy dielectrics with smooth boundaries.

Under the mentioned conditions, a hybrid solution based on the moment method and the physical optics approximation is obtained. In the solution the corrugations are replaced with polarization currents that are identical to those of the local tangential periodic corrugated surface, and the stratified cylinder is replaced with equivalent surface currents. New expressions for the equivalent physical-optics currents are employed which are more convenient than the standard ones.

It is shown that the bark layer and its roughness both reduce the radar cross section . At frequencies where the bark thickness and its roughness are considerable fractions of the wavelength the radar cross section reduction becomes very significant. It is also demonstrated that the corrugations can be replaced by an anisotropic layer and expressions for the elements of its permittivity tensor in terms of the corrugation parameters are derived In Appendix A. Application of the equivalent dielectric layer simplifies the problem extremely.

Contents

1 Introduction 1

2 Scattering from Periodic Corrugated Planar Dielectric Surface 2

2.1 Two-dimensional Green's Function for a Stratified Dielectric Half Space 3

2.2 Far Field Evaluation 6

2.3 Scattering from Inhomogeneous Periodic Dielectric Layer above a Half-Space Layered Medium 10

2.4 Numerical Implementation 14

3 High Frequency Scattering from Stratified Cylinders 19

4 Scattering from Corrugated Cylinder 26

5 Numerical Results 28

6 Conclusions 29

A APPENDIX A A-1

A1 Introduction A-1

A2 Theoretical Analysis A-2

A3 Low Frequency Approximation A-6

A4 Reflection Coefficient of Uniaxial Layered Medium A-7

A5 Numerical Examples A-12

List of Figures

1 Geometry of a periodic inhomogeneous dielectric layer over a stratified dielectric half-space. 3

2 Contour of integration and steepest descent path in γ-plane. 7

3 Geometry of the line source and its image. 9

4 Geometry of scattering problem of a stratified cylinder. 21

5 Normalized backscattering cross section $(\frac{\sigma}{\pi a})$ of a two-layer dielectric cylinder with $a = 10.5cm$, $a_1 = 10cm$, $\epsilon_1 = 15 + i7$, $\epsilon_2 = 4 + i1$ versus $k_0 a$ for TM case. 24

6 Normalized backscattering cross section $(\frac{\sigma}{\pi a})$ of a two-layer dielectric cylinder with $a = 10.5cm$, $a_1 = 10cm$, $\epsilon_1 = 15 + i7$, $\epsilon_2 = 4 + i1$ versus $k_0 a$ for TE case. 25

7 A corrugated cylinder geometry. 26

8 Geometry of the corrugated surface 33

9 Amplitude of the total induced current in the two-layer periodic corrugated surface versus incidence angle. 34

10 Phase of the total induced current in the two-layer periodic corrugated surface versus incidence angle. 35

11 Amplitude of the reflected field from the two-layer periodic corrugated surface versus incidence angle for E polarization. 36

12 Phase of the reflected field from the two-layer periodic corrugated surface versus incidence angle for E polarization. 37

13 Amplitude of the reflected field from the two-layer periodic corrugated surface versus incidence angle for H polarization. 38

14 Phase of the reflected field from the two-layer periodic corrugated surface versus incidence angle for H polarization. 39

15 The radar cross section of a corrugated cylinder for TM case with $a = 10.5\lambda_0$, $a_1 = 10\lambda_0$, $L = \lambda_0/4$, $\epsilon_1 = 4 + i1$, $\epsilon_2 = 15 + i7$, and $t = d = \lambda_0/8$ 40

16 The radar cross section of a corrugated cylinder for TE case with $a = 10.5\lambda_0$, $a_1 = 10\lambda_0$, $L = \lambda_0/4$, $\epsilon_1 = 4 + i1$, $\epsilon_2 = 15 + i7$, and $t = d = \lambda_0/8$ 41

17 The radar cross section of the corrugated cylinder for TE and TM cases using the numerical and the equivalent dielectric methods. . 42

A-1 An array of infinite dielectric slabs. A-2

A-2 Plane wave reflection from a stratified uniaxial dielectric half-space. A-7

A-3 Real part of the equivalent dielectric tensor elements for periodic slab medium with $L = \lambda_0/4$, $\epsilon = 4 + i1$, and $d/L = 0.5$ versus incidence angle; ϵ_x (H polarization), $\epsilon_y = \epsilon_z$ (E polarization). . . . A-15

A-4 Imaginary part of the equivalent dielectric tensor elements for periodic slab medium with $L = \lambda_0/4$, $\epsilon = 4 + i1$, and $d/L = 0.5$ versus incidence angle; ϵ_x (H polarization), $\epsilon_y = \epsilon_z$ (E polarization). . . . A-16

A-5 Real part of the equivalent dielectric tensor elements for a periodic slab medium with $L = \lambda_0/4$, $\epsilon = 4 + i1$, and $\phi_0 = 45°$ versus d/L; ϵ_x (H polarization), $\epsilon_y = \epsilon_z$ (E polarization). A-17

A-6 Imaginary part of the equivalent dielectric tensor elements for periodic slab medium with $L = \lambda_0/4$, $\epsilon = 4 + i1$, and $\phi_0 = 45°$ versus d/L; ϵ_x (H polarization), $\epsilon_y = \epsilon_z$ (E polarization). A-18

A-7 Location of zeros of (A-10)in the k_x^{II}-plane for for the periodic slab medium with $\epsilon = 4 + i1$, $\phi_0 = 45°$, $d/L = 0.5$, and (a) $L = 0.2\lambda_0$, (b) $L = 0.5\lambda_0$, (c) $L = 0.8\lambda_0$, (d) $L = 1.4\lambda_0$. A-19

A-8 Real part of the equivalent dielectric tensor elements for periodic slab medium with $\epsilon = 4 + i1$, and $\phi_0 = 45°$, and $d/L = 0,5$ versus L/λ_0; ϵ_x (H polarization), $\epsilon_y = \epsilon_z$ (E polarization). A-20

A-9 Imaginary part of the equivalent dielectric tensor elements for periodic slab medium with $\epsilon = 4 + i1$, and $\phi_0 = 45°$, and $d/L = 0,5$ versus L/λ_0; ϵ_x (H polarization), $\epsilon_y = \epsilon_z$ (E polarization). A-21

A-10 Amplitude of reflection coefficient of a corrugated surface for both E and H polarizations versus incidence angle; $L = 0.25\lambda_0$. A-22

A-11 Phase of reflection coefficient of a corrugated surface for both E and H polarizations versus incidence angle; $L = 0.25\lambda_0$. A-23

A-12 Amplitude of reflection coefficient of a corrugated surface for both E and H polarizations versus incidence angle; $L = 0.4\lambda_0$. A-24

A-13 Phase of reflection coefficient of a corrugated surface for both E and H polarizations versus incidence angle; $L = 0.4\lambda_0$. A-25

A-14 Geometry of a wedge-shape microwave absorber and its staircase approximation. A-26

A-15 Amplitude of reflection coefficient of a wedge-shape microwave absorber for both E and H polarizations versus incidence angle; $L = 0.4\lambda_0$, $H = 1.5\lambda_0$, $D = 1\lambda_0$, and $\epsilon = 2.5 + i0.5$. A-27

1 Introduction

The literature concerning the problem of scattering from cylinders with rough surfaces is relatively scarce. To our knowledge the first treatment of a problem of this sort was given by Clemmow [1959] where a perturbation solution to an eigen function-expansion was obtained for a perfectly conducting cylinder with almost circular cross section, and only the E polarization case was considered. This technique is restricted to very smooth and small roughness functions. Other perturbation techniques for perfectly conducting cylinders with very small roughness have also been developed [Cabayan and Murphy, 1973; Tong 1974]. None of the existing techniques can handle dielectric rough cylinders, particularly when the roughness height is on the order of the wavelength.

Study of this problem is motivated by the fact that a tree trunk can be viewed as a multi-layer dielectric cylinder with a rough outer layer. The outer layer has almost a periodic pattern and the roughness height is proportional to the diameter of the cylinder. This layer consists of dead cells with almost no water content; hence, its dielectric constant is low and slightly lossy. The inner layers that carry high dielectric fluids have very high and lossy dielectric constants. In modeling a tree, the branches and trunk usually are considered to be homogeneous smooth cylinders [Durden et al, 1988; Karam and Fung,1988]. In this report the effect of bark and its roughness on scattering is studied.

Under the assumption that the bark roughness is a regular corrugation in only the angular direction (i.e., ignoring variations in the axial direction) and the radius

of curvature of the cylinder is much larger than the wavelength and the period of corrugation, an approximate solution to the scattering problem is obtained. In this solution, each point on the surface of the cylinder is approximated by its tangential plane. Then the polarization current in the periodic tangential surface is obtained numerically. Once the polarization current in the corrugations is found, the scattered field due to the corrugations together with the scattered field from the smooth cylinder (when the corrugation is removed) give rise to the total scattered field. The scattered field for a smooth cylinder is obtained using new physical optics surface currents that are more convenient than the traditional ones. It is shown that the corrugation on the surface can be replaced with an anisotropic layer which would extremely simplifies the problem. In Appendix A the equivalent dielectric tensor of the corrugated layer in terms of the corrugation parameters is derived.

2 Scattering from Periodic Corrugated Planar Dielectric Surface

In this section we seek a numerical solution for the total field (or polarization current) inside a periodic inhomogeneous layer lying over a stratified dielectric half-space illuminated by a plane wave. The geometry of the scattering problem is shown in Fig. 1. First the two-dimensional Green's function for a stratified dielectric medium is found. Using Floquet's theorem these results are extended to the periodic case. Then the problem will be formulated as an integral equation

that can be solved numerically by the method of moments.

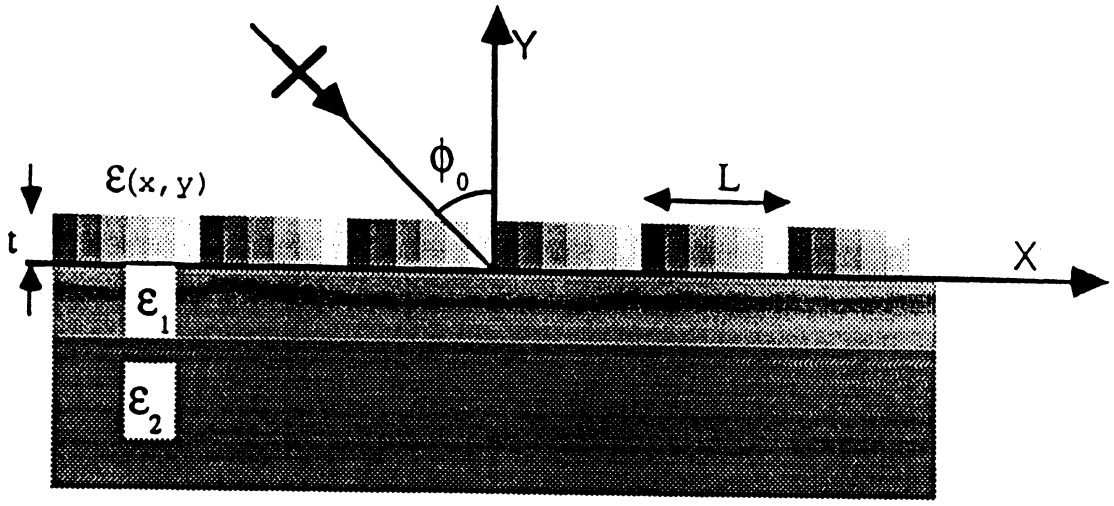

Figure 1: Geometry of a periodic inhomogeneous dielectric layer over a stratified dielectric half-space.

2.1 Two-dimensional Green's Function for a Stratified Dielectric Half Space

For a volume distribution of electric current ($\mathbf{J}_e$) occupying region V in free space, the corresponding Hertz vector is given by

$$\mathbf{\Pi} = \frac{iZ_0}{4\pi k_0}\int_V \mathbf{J}(\bar{r}')\frac{e^{ik_0|\bar{r}-\bar{r}'|}}{|\bar{r}-\bar{r}'|}\mathrm{dv}',$$

where $Z_0(=\frac{1}{Y_0})$ is the free-space characteristic impedance and the resulting fields are

$$\begin{aligned} E_x &= k_0^2\left(1+\tfrac{1}{k_0^2}\tfrac{\partial^2}{\partial x^2}\right)\Pi_x + \tfrac{\partial^2}{\partial x\partial y}\Pi_y \\ E_y &= \tfrac{\partial^2}{\partial y\partial x}\Pi_x + k_0^2\left(1+\tfrac{1}{k_0^2}\tfrac{\partial^2}{\partial y^2}\right)\Pi_y \\ E_z &= k_0^2\Pi_z \end{aligned} \qquad (1)$$

The Hertz vector potential associated with an infinite current filament located at point (x', y') in free space with amplitude I_p and orientation $\hat{p}$ is of the form

$$\Pi_p(x,y) = \frac{-Z_0}{4k_0} H_0^{(1)}(k_0\sqrt{(x-x')^2+(y-y')^2})I_p \qquad p = x, y \text{ or } z. \tag{2}$$

The corresponding field components can be obtained by inserting (2) into (1) and then by employing the identity

$$H_0^{(1)}(k_0\sqrt{(x-x')^2+(y-y')^2}) = \frac{1}{\pi}\int_{-\infty}^{+\infty} \frac{e^{ik_y|y-y'|-ik_x(x-x')}}{k_y} \mathrm{d}k_x \tag{3}$$

the resulting fields can be expressed in terms of continuous spectrum of plane waves. In (3) $k_y = \sqrt{k_0^2 - k_x^2}$ and the branch of the square root is chosen such that $\sqrt{-1} = i$.

In the presence of the dielectric half-space, when the current filament is in the upper half-space, each plane wave, is reflected at the air-dielectric interface according to Fresnel's law. It should be noted that the incidence angle of each plane wave, in general, is complex and is given by

$$\gamma = \arctan(\frac{k_x}{k_y}).$$

The net effect of the dielectric half-space on the radiated field can be obtained by superimposing all of the reflected plane waves that are of the following form

$$R_q(\gamma)e^{ik_y(y+y')-ik_x(x-x')}, \qquad q = E \text{ or } H.$$

where $R_q(\gamma)$ is the Fresnel reflection coefficient. The total reflected field can now be obtained by noting that

$$E_x^r = -R_H(\gamma)E_x^i$$

$$E_y^r = R_H(\gamma)E_y^i$$

$$E_z^r = R_E(\gamma)E_z^i$$

and since the direction of propagation along the y axis is reversed for the reflected waves, the operator $\frac{\partial}{\partial y}$ for the x and y components of the reflected field must be replaced by $-\frac{\partial}{\partial y}$. Thus,

$$\begin{aligned}
E_x^r &= -\tfrac{k_0 Z_0}{4\pi}[-I_x(1+\tfrac{1}{k_0^2}\tfrac{\partial^2}{\partial x^2}) + I_y\tfrac{1}{k_0^2}\tfrac{\partial^2}{\partial x\partial y}]\textstyle\int_{-\infty}^{+\infty} R_H(\gamma)\tfrac{e^{ik_y(y+y')-ik_x(x-x')}}{k_y}\mathrm{d}k_x,\\
E_y^r &= -\tfrac{k_0 Z_0}{4\pi}[-I_x\tfrac{1}{k_0^2}\tfrac{\partial^2}{\partial y\partial x} + I_y(1+\tfrac{1}{k_0^2}\tfrac{\partial^2}{\partial y^2})]\textstyle\int_{-\infty}^{+\infty} R_H(\gamma)\tfrac{e^{ik_y(y+y')-ik_x(x-x')}}{k_y}\mathrm{d}k_x, \qquad (4)\\
E_z^r &= -\tfrac{k_0 Z_0}{4\pi}I_z\textstyle\int_{-\infty}^{+\infty} R_E(\gamma)\tfrac{e^{ik_y(y+y')-ik_x(x-x')}}{k_y}\mathrm{d}k_x.
\end{aligned}$$

In matrix notation the total field in the upper half-space can be represented by

$$\mathbf{E} = \begin{bmatrix} G_{xx} & G_{xy} & 0 \\ G_{yx} & G_{yy} & 0 \\ 0 & 0 & G_{zz} \end{bmatrix}\begin{bmatrix} I_x \\ I_y \\ I_z \end{bmatrix}, \qquad (5)$$

where

$$\begin{aligned}
G_{xx} = &-\tfrac{k_0 Z_0}{4}(1+\tfrac{1}{k_0^2}\tfrac{\partial^2}{\partial x^2})[H_0^{(1)}(k_0\sqrt{(x-x')^2+(y-y')^2})\\
&-\tfrac{1}{\pi}\textstyle\int_{-\infty}^{+\infty} R_H(\gamma)\tfrac{e^{ik_y(y+y')-ik_x(x-x')}}{k_y}\mathrm{d}k_x],
\end{aligned}$$

$$\begin{aligned}
G_{xy} = &-\tfrac{Z_0}{4k_0}\tfrac{\partial^2}{\partial x\partial y}[H_0^{(1)}(k_0\sqrt{(x-x')^2+(y-y')^2})\\
&+\tfrac{1}{\pi}\textstyle\int_{-\infty}^{+\infty} R_H(\gamma)\tfrac{e^{ik_y(y+y')-ik_x(x-x')}}{k_y}\mathrm{d}k_x], \qquad (6)
\end{aligned}$$

$$\begin{aligned}
G_{yx} = &-\tfrac{Z_0}{4k_0}\tfrac{\partial^2}{\partial y\partial x}[H_0^{(1)}(k_0\sqrt{(x-x')^2+(y-y')^2})\\
&-\tfrac{1}{\pi}\textstyle\int_{-\infty}^{+\infty} R_H(\gamma)\tfrac{e^{ik_y(y+y')-ik_x(x-x')}}{k_y}\mathrm{d}k_x],
\end{aligned}$$

$$G_{yy} = -\frac{k_0 Z_0}{4}(1+\frac{1}{k_0^2}\frac{\partial^2}{\partial y^2})[H_0^{(1)}(k_0\sqrt{(x-x')^2+(y-y')^2}) + \frac{1}{\pi}\int_{-\infty}^{+\infty} R_H(\gamma)\frac{e^{ik_y(y+y')-ik_x(x-x')}}{k_y}\mathrm{d}k_x],$$

$$G_{zz} = -\frac{k_0 Z_0}{4}[H_0^{(1)}(k_0\sqrt{(x-x')^2+(y-y')^2}) + \frac{1}{\pi}\int_{-\infty}^{+\infty} R_E(\gamma)\frac{e^{ik_y(y+y')-ik_x(x-x')}}{k_y}\mathrm{d}k_x]$$

are the elements of the dyadic Green's function for two-dimensional layered dielectric half-space problems. If an electric current distribution $\mathbf{J}_e$ occupies region S in the upper half-space, the radiated electric field at any point in the upper half-space can be obtained from:

$$\begin{aligned} E_x^s(x,y) &= \int_S [G_{xx}(x,y;x',y')J_x(x',y') + G_{xy}(x,y;x',y')J_y(x',y')]\mathrm{d}x'\mathrm{d}y' \\ E_y^s(x,y) &= \int_S [G_{yx}(x,y;x',y')J_x(x',y') + G_{yy}(x,y;x',y')J_y(x',y')]\mathrm{d}x'\mathrm{d}y' \\ E_z^s(x,y) &= \int_S G_{zz}(x,y;x',y')J_z(x',y')\mathrm{d}x'\mathrm{d}y' \end{aligned} \tag{7}$$

2.2 Far Field Evaluation

In scattering problems the quantity of interest usually is the far field expression. Here we derive the approximate form of the Green's function in the far zone using the saddle-point technique. All the elements of the dyadic Green's function have an integral of the form

$$I = \frac{1}{\pi}\int_{-\infty}^{+\infty} R_q(\gamma)\frac{e^{ik_y(y+y')-ik_x(x-x')}}{k_y}\mathrm{d}k_x \tag{8}$$

Using the standard change of variable

$$k_x = k_0 \sin\gamma$$

the integration contour is changed from the real axis in the complex k_x-plane to contour Γ in γ-plane as shown in Fig. 2. Also by defining

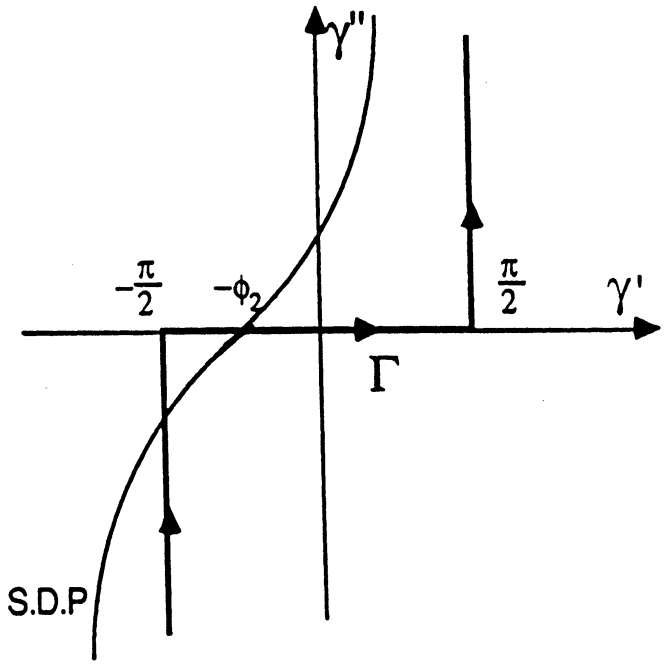

Figure 2: Contour of integration and steepest descent path in γ-plane.

$$x - x' = \rho_2 \sin\phi_2, \qquad y - y' = \rho_2 \cos\phi_2$$

integral (8) in γ-plane becomes:

$$I = \frac{1}{\pi} \int_\Gamma R_q(\gamma) e^{ik_0\rho_2 \cos(\gamma+\phi_2)} d\gamma$$

The saddle point is the solution of

$$\frac{\mathrm{d}}{\mathrm{d}\gamma} \cos(\gamma + \phi_2) = 0$$

implies $\gamma = -\phi_2$. When $k_0\rho_2 \gg 1$ the approximate value of I can be obtained by deforming the contour of integration from Γ to the steepest descent path (S.D.P.) given by

$$\mathrm{Im}[i\cos(\gamma + \phi_2)] = 1.$$

There are some poles associated with the reflection coefficient function ($R_q(\gamma)$) of a layered dielectric medium that are captured when the contour is deformed. the contribution of these poles gives rise to surface waves, but their effect can be ignored if the dielectric materials are lossy and observation point is away from the interface. Under these conditions we get

$$\begin{aligned} I &= \tfrac{1}{\pi} R_q(-\phi_2) \int_{S.D.P.} e^{ik_0\rho_2\cos(\gamma+\phi_2)} \mathrm{d}\gamma \\ &\approx \sqrt{\tfrac{2}{\pi k_0\rho_2}} e^{i(k_0\rho_2 - \pi/4)} R_q(\phi_2), \end{aligned}$$

where we have used the fact that R_q is an even function. Also the large argument expansion of the Hankel function can be used for distant approximations, i.e.

$$H_0^{(1)}(k_0\sqrt{(x-x')^2 + (y-y')^2}) \approx \sqrt{\frac{2}{\pi k_0\rho_1}} e^{i(k_0\rho_1 - \pi/4)},$$

where $\rho_1 = \sqrt{(x-x')^2 + (y-y')^2}$. From Fig. 3 it is seen that in the far zone the following approximations can be used also

$$\begin{aligned} \phi_1 &= \phi_2 = \phi, \\ \rho_1 &= \rho - x'\sin\phi - y'\cos\phi, \\ \rho_2 &= \rho - x'\sin\phi + y'\cos\phi. \end{aligned}$$

These approximations can be inserted into expressions for the dyadic Green's function given by (6). The far field approximation of derivatives of the Hankel function

and integral I can be obtained by retaining the terms up to the order $\rho^{-1/2}$ and discarding the rest. Thus the expressions for the Green's function elements in the far zone become:

$$
\begin{aligned}
G_{xx} &= -\frac{k_0 Z_0}{4}\sqrt{\frac{2}{\pi k_0 \rho}}e^{i(k_0\rho-\pi/4)}\cos^2\phi e^{-ik_0\sin\phi x'}[e^{-ik_0\cos\phi y'} - R_H(\phi)e^{ik_0\cos\phi y'}] \\
G_{xy} &= \frac{k_0 Z_0}{4}\sqrt{\frac{2}{\pi k_0 \rho}}e^{i(k_0\rho-\pi/4)}\sin\phi\cos\phi e^{-ik_0\sin\phi x'}[e^{-ik_0\cos\phi y'} + R_H(\phi)e^{ik_0\cos\phi y'}] \\
G_{yx} &= \frac{k_0 Z_0}{4}\sqrt{\frac{2}{\pi k_0 \rho}}e^{i(k_0\rho-\pi/4)}\sin\phi\cos\phi e^{-ik_0\sin\phi x'}[e^{-ik_0\cos\phi y'} - R_H(\phi)e^{ik_0\cos\phi y'}] \\
G_{yy} &= -\frac{k_0 Z_0}{4}\sqrt{\frac{2}{\pi k_0 \rho}}e^{i(k_0\rho-\pi/4)}\sin^2\phi e^{-ik_0\sin\phi x'}[e^{-ik_0\cos\phi y'} + R_H(\phi)e^{ik_0\cos\phi y'}] \\
G_{zz} &= -\frac{k_0 Z_0}{4}\sqrt{\frac{2}{\pi k_0 \rho}}e^{i(k_0\rho-\pi/4)}e^{-ik_0\sin\phi x'}[e^{-ik_0\cos\phi y'} + R_E(\phi)e^{ik_0\cos\phi y'}].
\end{aligned}
\tag{9}
$$

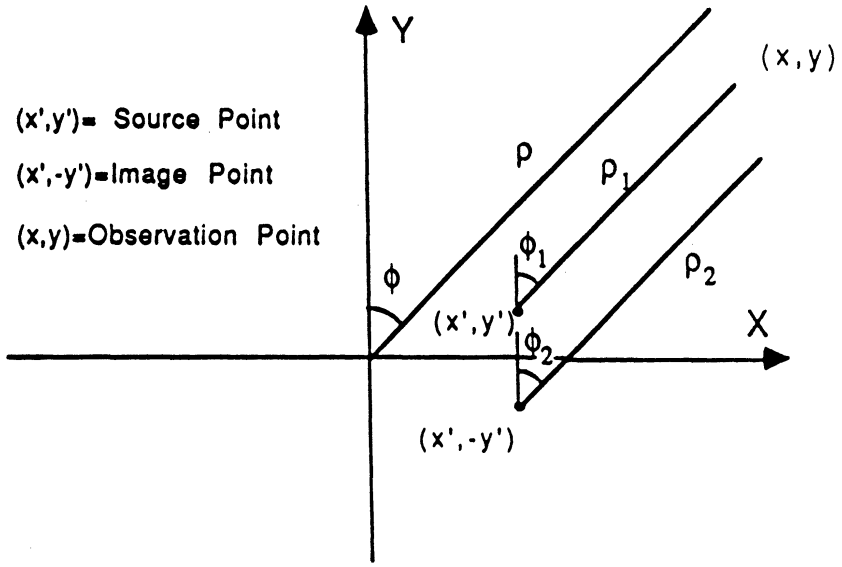

Figure 3: Geometry of the line source and its image.

It can easily be shown that for an electric current distribution $\mathbf{J}_e$ the radiated far field does not have a $\hat{\rho}$ component and the far field amplitude defined by

$$\mathbf{E} = \sqrt{\frac{2}{\pi k_0 \rho}}e^{i(k_0\rho-\pi/4)}\mathbf{S}$$

has components

$$
\begin{aligned}
S_\phi = \; & \tfrac{k_0 Z_0}{4}\{\textstyle\int_S \cos\phi J_x(x',y')e^{-ik_0\sin\phi x'}[e^{-ik_0\cos\phi y'} - R_H(\phi)e^{ik_0\cos\phi y'}]\mathrm{d}x'\mathrm{d}y' \\
& - \textstyle\int_S \sin\phi J_y(x',y')e^{-ik_0\sin\phi x'}[e^{-ik_0\cos\phi y'} + R_H(\phi)e^{ik_0\cos\phi y'}]\mathrm{d}x'\mathrm{d}y'\}, \qquad (10) \\
S_z = \; & -\tfrac{k_0 Z_0}{4}\textstyle\int_S J_z(x',y')e^{-ik_0\sin\phi x'}[e^{-ik_0\cos\phi y'} + R_E(\phi)e^{ik_0\cos\phi y'}]\mathrm{d}x'\mathrm{d}y',
\end{aligned}
$$

2.3 Scattering from Inhomogeneous Periodic Dielectric Layer above a Half-Space Layered Medium

Consider an inhomogeneous dielectric layer of thickness t on top of a stratified half-space dielectric medium as shown in Fig. 1. The permittivity of the inhomogeneous layer is represented by $\epsilon(x,y)$ which is a periodic function of x with period L. Suppose this structure is illuminated by a plane wave whose angle of incidence and polarization respectively are ϕ_0 and $\hat{p}$. For an E-polarized wave $\hat{p} = \hat{z}$ and for an H-polarized wave $\hat{p} = -\cos\phi_0\hat{x} - \sin\phi_0\hat{y}$, thus the incident wave may be represented by

$$\mathbf{E}^i = \hat{p}e^{ik_0(\sin\phi_0 x - \cos\phi_0 y)}. \qquad (11)$$

A polarization current distribution is induced in the inhomogeneous layer. This current gives rise to a scattered field that can be obtained from (7). The polarization current is proportional to the total field within the inhomogeneous layer. The total field is comprised of the incident field, the reflected field which would have existed in the absence of the inhomogeneous layer, and the scattered field, i.e.

$$\mathbf{E}^t = \mathbf{E}^i + \mathbf{E}^r + \mathbf{E}^s.$$

The polarization current in terms of the total field is given by

$$\mathbf{J}_e(x,y) = -ik_0 Y_0(\epsilon(x,y)-1)\mathbf{E}^t. \tag{12}$$

Upon substitution of expression (7) for $\mathbf{E}^s$ into (12) a set of integral equations for polarization current can be obtained; for E polarization we have

$$\begin{aligned} J_z(x,y) = \; & -ik_0 Y_0(\epsilon(x,y)-1)\{e^{ik_0 \sin\phi_0 x}[e^{-ik_0\cos\phi_0 y} + R_E(\phi_0)e^{ik_0\cos\phi_0 y}] \\ & + \int_0^t \int_{-\infty}^{+\infty} J_z(x',y')G_{zz}(x,y;x',y')\mathrm{d}x'\mathrm{d}y'\}, \end{aligned} \tag{13}$$

and for H polarization

$$\begin{aligned} J_x(x,y) = \; & -ik_0 Y_0(\epsilon(x,y)-1)\{\cos\phi_0 e^{ik_0\sin\phi_0 x}[-e^{-ik_0\cos\phi_0 y} + R_H(\phi_0)e^{ik_0\cos\phi_0 y}] \\ & + \int_0^t \int_{-\infty}^{+\infty}[J_x(x',y')G_{xx}(x,y;x',y') + J_y(x',y')G_{xy}(x,y;x',y')]\mathrm{d}x'\mathrm{d}y'\}, \\ J_y(x,y) = \; & -ik_0 Y_0(\epsilon(x,y)-1)\{-\sin\phi_0 e^{ik_0\sin\phi_0 x}[e^{-ik_0\cos\phi_0 y} + R_H(\phi_0)e^{ik_0\cos\phi_0 y}] \\ & + \int_0^t \int_{-\infty}^{+\infty}[J_x(x',y')G_{yx}(x,y;x',y') + J_y(x',y')G_{yy}(x,y;x',y')]\mathrm{d}x'\mathrm{d}y'\}. \end{aligned} \tag{14}$$

Since there is no closed-form representation for the kernel of these integral equations, finding the solution, even numerically, seems impossible. But by employing Floquet's theorem the integral equations can be reduced to a form which is amenable to numerical solution. The fact that the permittivity of the inhomogeneous layer is periodic in x,excluding a phase factor, all the field quantities are required to be periodic in x . Therefore the polarization current must satisfy

$$\mathbf{J}_e(x+nL,y) = \mathbf{J}_e(x,y)e^{ik_0\sin\phi_0 nL} \tag{15}$$

Now by using (15) the integration with respect to x can be simplified significantly by breaking the integral into multiples of a period, that is

$$\begin{aligned} I_{zz} &= \int_{-\infty}^{+\infty} G_{zz}(x,y;x',y')J_z(x',y')\mathrm{d}x'\mathrm{d}y' \\ &= \sum_{n=-\infty}^{+\infty} \int_{x_0+nL}^{x_0+(n+1)L} G_{zz}(x,y;x',y')J_z(x',y')\mathrm{d}x'\mathrm{d}y' \end{aligned} \tag{16}$$

At this stage, if the variable x' is changed to $x'+nL$ and property (15) is used, I_{zz} becomes

$$I_{zz} = \int_{x_0}^{x_0+L} G_{zz}^{p}(x,y;x',y')J_z(x',y')\mathrm{d}x'\mathrm{d}y'$$

where

$$G_{zz}^{p}(x,y;x',y') = \sum_{n=-\infty}^{+\infty} G_{zz}(x,y;x'+nL,y')e^{ik_0\sin\phi_0 nL}$$

If the expression for G_{zz} as given by (6) is inserted in the above equation and the order of summation and integration is interchanged, and then the identity

$$\sum_{n=-\infty}^{+\infty} e^{inL(k_0\sin\phi_0+k_x)} = 2\pi \sum_{n=-\infty}^{+\infty} \delta[(k_x+k_0\sin\phi_0)L-2\pi n]$$

is employed, the periodic Green's function simplifies to

$$G_{zz}^{p}(x,y;x',y') = -\frac{k_0 Z_0}{2L}\sum_{n=-\infty}^{+\infty}[e^{ik_{ny}|y-y'|}+R_E(\gamma_n)e^{ik_{ny}(y+y')}]\frac{e^{-ik_{nx}(x-x')}}{k_{ny}} \tag{17}$$

where

$$k_{nx} = \frac{2\pi n}{L} - k_0\sin\phi_0, \qquad k_{ny} = \sqrt{k_0^2-k_{nx}^2},$$

and

$$\gamma_n = \arctan(\frac{k_{nx}}{k_{ny}}).$$

Other elements of the periodic Green's function can also be obtained in the same manner

$$
\begin{aligned}
G^p_{xx}(x,y;x',y') &= -\frac{k_0 Z_0}{2L}\left(1+\frac{1}{k_0^2}\frac{\partial^2}{\partial x^2}\right)\sum_{n=-\infty}^{+\infty}\left[e^{ik_{ny}|y-y'|}-R_H(\gamma_n)e^{ik_{ny}(y+y')}\right]\frac{e^{-ik_{nx}(x-x')}}{k_{ny}} \\
G^p_{xy}(x,y;x',y') &= -\frac{Z_0}{2Lk_0}\frac{\partial^2}{\partial x\partial y}\sum_{n=-\infty}^{+\infty}\left[e^{ik_{ny}|y-y'|}+R_H(\gamma_n)e^{ik_{ny}(y+y')}\right]\frac{e^{-ik_{nx}(x-x')}}{k_{ny}} \\
G^p_{yx}(x,y;x',y') &= -\frac{Z_0}{2Lk_0}\frac{\partial^2}{\partial y\partial x}\sum_{n=-\infty}^{+\infty}\left[e^{ik_{ny}|y-y'|}-R_H(\gamma_n)e^{ik_{ny}(y+y')}\right]\frac{e^{-ik_{nx}(x-x')}}{k_{ny}} \\
G^p_{yy}(x,y;x',y') &= -\frac{k_0 Z_0}{2L}\left(1+\frac{1}{k_0^2}\frac{\partial^2}{\partial y^2}\right)\sum_{n=-\infty}^{+\infty}\left[e^{ik_{ny}|y-y'|}+R_H(\gamma_n)e^{ik_{ny}(y+y')}\right]\frac{e^{-ik_{nx}(x-x')}}{k_{ny}}.
\end{aligned}
\tag{18}
$$

The integral equations (13) and (14) now take the following form

$$
\begin{aligned}
J_z(x,y) = \; & -ik_0Y_0(\epsilon(x,y)-1)\{e^{ik_0\sin\phi_0 x}[e^{-ik_0\cos\phi_0 y}+R_E(\phi_0)e^{ik_0\cos\phi_0 y}] \\
& +\int_0^t\int_{-L/2}^{+L/2} J_z(x',y')G^p_{zz}(x,y;x',y')\mathrm{d}x'\mathrm{d}y'\}, \\
J_x(x,y) = \; & -ik_0Y_0(\epsilon(x,y)-1)\{\cos\phi_0 e^{ik_0\sin\phi_0 x}[-e^{-ik_0\cos\phi_0 y}+R_H(\phi_0)e^{ik_0\cos\phi_0 y}] \\
& +\int_0^t\int_{-L/2}^{+L/2} [J_x(x',y')G^p_{xx}(x,y;x',y')+J_y(x',y')G^p_{xy}(x,y;x',y')]\mathrm{d}x'\mathrm{d}y'\}, \\
J_y(x,y) = \; & -ik_0Y_0(\epsilon(x,y)-1)\{-\sin\phi_0 e^{ik_0\sin\phi_0 x}[e^{-ik_0\cos\phi_0 y}+R_H(\phi_0)e^{ik_0\cos\phi_0 y}] \\
& +\int_0^t\int_{-L/2}^{+L/2} [J_x(x',y')G^p_{yx}(x,y;x',y')+J_y(x',y')G^p_{yy}(x,y;x',y')]\mathrm{d}x'\mathrm{d}y'\}.
\end{aligned}
\tag{19}
$$

Far away from the surface ($y \gg \lambda_0$), contribution of only a few terms of the summations in (18) are observable. These terms correspond to values of n such that k_{ny} is real and they are known as the Bragg modes. Among all the Bragg modes the mode corresponding to $n = 0$ carries most of the scattered energy and this is specifically true when $L < \lambda_0$. The scattered field due to this mode is a

plane wave and for E and H Polarization, respectively, we have

$$\mathbf{E}_E = \frac{-Z_0}{2L\cos\phi_0}\left\{\int_0^t\int_{-L/2}^{+L/2} J_z(x',y')[e^{-ik_0\cos\phi_0 y'} + R_E e^{ik_0\cos\phi_0 y'}]e^{-ik_0\sin\phi_0 x'}\mathrm{d}x'\mathrm{d}y'\right\} \cdot e^{ik_0(\cos\phi_0 y+\sin\phi_0 x)}\hat{z} \tag{20}$$

$$\mathbf{E}_H = -\frac{Z_0}{2L\cos\phi_0}\left\{\cos\phi_0\int_0^t\int_{-L/2}^{+L/2} J_x(x',y')[e^{-ik_0\cos\phi_0 y'} - R_H e^{ik_0\cos\phi_0 y'}]e^{-ik_0\sin\phi_0 x'}\mathrm{d}x'\mathrm{d}y' - \sin\phi_0\int_0^t\int_{-L/2}^{+L/2} J_y(x',y')[e^{-ik_0\cos\phi_0 y'} + R_H e^{ik_0\cos\phi_0 y'}]e^{-ik_0\sin\phi_0 x'}\mathrm{d}x'\mathrm{d}y'\right\} \cdot(\cos\phi_0\hat{x} - \sin\phi_0\hat{y})e^{ik_0(\cos\phi_0 y+\sin\phi_0 x)} \tag{21}$$

2.4 Numerical Implementation

It is very unlikely to find an analytical solution to the equations as given by (19) even for the simplest form of $\epsilon(x,y)$. However an approximate numerical solution can be obtained using the standard moment method with point matching technique. In this method the cross section of the inhomogeneous layer over one period is discretized into small rectangular segments over which the dielectric constant and polarization current can be assumed to be constant. Now in equation (19) the integrals over one period of the inhomogeneous layer can be broken up into summation of integrals over each segment where the polarization current is constant.

Let pq designate a cell whose center coordinate is $(x_p, y_q) = (p\Delta x, q\Delta y)$, where p and q are some integers and Δx and Δy are dimensions of the rectangular segments. If the polarization currents as given by (19) are evaluated at the center of uv-cell (point matching) the integral equations can be cast into matrix equations.

The matrices formed by this technique are known as the impedance matrices. The solution to this matrix equation gives the polarization current at the center of each segment.

After a simple integration of the periodic Green's functions over the area of pq-cell, it can be shown that the entries of the impedance matrix for E polarization (TM case) are of the form

$$Z(u,v;p,q) = \begin{cases} \frac{2ik_0^2}{L}(\epsilon(u,v)-1)\sum\limits_{n=-\infty}^{+\infty}[e^{ik_{ny}|y_v-y_q|}+R_E(\gamma_n)e^{ik_{ny}(y_v+y_q)}]\frac{\sin(k_{ny}\Delta y/2)}{k_{nx}k_{ny}^2} \\ \quad \cdot \sin(k_{nx}\Delta x/2)e^{-ik_{nx}(x_u-x_p)} & v \neq q \\ \frac{2ik_0^2}{L}(\epsilon(u,v)-1)\sum\limits_{n=-\infty}^{+\infty}[-ie^{ik_{ny}\Delta y/2}+i+R_E(\gamma_n)e^{i2k_{ny}y_v} \\ \quad \cdot \sin(k_{ny}\Delta y/2)]\frac{1}{k_{nx}k_{ny}^2}\sin(k_{nx}\Delta x/2)e^{-ik_{nx}(x_u-x_p)} & v = q \; u \neq p \\ -1+\frac{2ik_0^2}{L}(\epsilon(u,v)-1)\sum\limits_{n=-\infty}^{+\infty}[-ie^{ik_{ny}\Delta y/2}+i+R_E(\gamma_n)e^{i2k_{ny}y_v} \\ \quad \cdot \sin(k_{ny}\Delta y/2)]\frac{1}{k_{nx}k_{ny}^2}\cdot\sin(k_{nx}\Delta x/2) & v = q \; u = p. \end{cases} \tag{22}$$

For H polarization (TE case) the integral equations for J_x and J_y are coupled, which result in coupled matrix equations that can be combined into a single matrix equation. The resultant impedance matrix consists of four sub-matrices of the following form

$$\mathcal{Z} = \begin{bmatrix} \mathcal{Z}_1 & \mathcal{Z}_2 \\ \mathcal{Z}_3 & \mathcal{Z}_4 \end{bmatrix},$$

whose entries are given by

$$Z_1(u,v;p,q) = \begin{cases} \frac{2ik_0^2}{L}(\epsilon(u,v)-1)\sum_{n=-\infty}^{+\infty}[e^{ik_{ny}|y_v-y_q|} - R_H(\gamma_n)e^{ik_{ny}(y_v+y_q)}]\frac{(1-k_{nx}^2/k_0^2)}{k_{nx}k_{ny}^2} \\ \quad \cdot \sin(k_{ny}\Delta y/2)\sin(k_{nx}\Delta x/2)e^{-ik_{nx}(x_u-x_p)} \qquad v \neq q \\ \frac{2ik_0^2}{L}(\epsilon(u,v)-1)\sum_{n=-\infty}^{+\infty}[-ie^{ik_{ny}\Delta y/2} + i - R_H(\gamma_n)e^{i2k_{ny}y_v} \\ \quad \cdot \sin(k_{ny}\Delta y/2)]\frac{(1-k_{nx}^2/k_0^2)}{k_{nx}k_{ny}^2}\sin(k_{nx}\Delta x/2)e^{-ik_{nx}(x_u-x_p)} \\ \qquad\qquad\qquad\qquad\qquad\qquad v = q \; u \neq p \\ -1 + \frac{2ik_0^2}{L}(\epsilon(u,v)-1)\sum_{n=-\infty}^{+\infty}[-ie^{ik_{ny}\Delta y/2} + i - R_H(\gamma_n)e^{i2k_{ny}y_v} \\ \quad \cdot \sin(k_{ny}\Delta y/2)]\frac{(1-k_{nx}^2/k_0^2)}{k_{nx}k_{ny}^2} \cdot \sin(k_{nx}\Delta x/2) \qquad v = q \; u = p, \end{cases} \tag{23}$$

$$Z_2(u,v;p,q) = \begin{cases} \frac{2i}{L}(\epsilon(u,v)-1)\sum_{n=-\infty}^{+\infty}[\mathrm{sgn}(y_v-y_q)e^{ik_{ny}|y_v-y_q|} + R_H(\gamma_n)e^{ik_{ny}(y_v+y_q)}] \\ \quad \cdot \frac{1}{k_{ny}}\sin(k_{ny}\Delta y/2)\sin(k_{nx}\Delta x/2)e^{-ik_{nx}(x_u-x_p)} \qquad v \neq q \\ \frac{2i}{L}(\epsilon(u,v)-1)\sum_{n=-\infty}^{+\infty}R_H(\gamma_n)e^{i2k_{ny}y_v}\sin(k_{ny}\Delta y/2)\frac{1}{k_{ny}} \\ \quad \cdot \sin(k_{nx}\Delta x/2)e^{-ik_{nx}(x_u-x_p)} \qquad v = q, \end{cases} \tag{24}$$

$$Z_3(u,v;p,q) = \begin{cases} \frac{2i}{L}(\epsilon(u,v)-1)\sum_{n=-\infty}^{+\infty}[\mathrm{sgn}(y_v-y_q)e^{ik_{ny}|y_v-y_q|} - R_H(\gamma_n)e^{ik_{ny}(y_v+y_q)}] \\ \quad \cdot \frac{1}{k_{ny}}\sin(k_{ny}\Delta y/2)\sin(k_{nx}\Delta x/2)e^{-ik_{nx}(x_u-x_p)} \qquad v \neq q \\ \frac{2i}{L}(\epsilon(u,v)-1)\sum_{n=-\infty}^{+\infty}-R_H(\gamma_n)e^{i2k_{ny}y_v}\sin(k_{ny}\Delta y/2)\frac{1}{k_{ny}} \\ \quad \cdot \sin(k_{nx}\Delta x/2)e^{-ik_{nx}(x_u-x_p)} \qquad v = q, \end{cases} \tag{25}$$

$$Z_4(u,v;p,q) = \begin{cases} \frac{2ik_0^2}{L}(\epsilon(u,v)-1)\sum\limits_{n=-\infty}^{+\infty}\{(1-\frac{k_{ny}^2}{k_0^2})[e^{ik_{ny}|y_v-y_q|}+R_H(\gamma_n)e^{ik_{ny}(y_v+y_q)}] \\ \quad \frac{1}{k_{nx}k_{ny}^2}\cdot\sin(k_{ny}\Delta y/2)\sin(k_{nx}\Delta x/2)e^{-ik_{nx}(x_u-x_p)}\} \qquad v\neq q \\ \frac{2ik_0^2}{L}(\epsilon(u,v)-1)\sum\limits_{n=-\infty}^{+\infty}[-i(1-\frac{k_{ny}^2}{k_0^2})e^{ik_{ny}\Delta y/2}+i+R_H(\gamma_n)(1-\frac{k_{ny}^2}{k_0^2}) \\ \quad \cdot\sin(k_{ny}\Delta y/2)e^{i2k_{ny}y_v}]\frac{1}{k_{nx}k_{ny}^2}\sin(k_{nx}\Delta x/2)e^{-ik_{nx}(x_u-x_p)} \\ \qquad\qquad v=q\ u\neq p \\ -1+\frac{2ik_0^2}{L}(\epsilon(u,v)-1)\sum\limits_{n=-\infty}^{+\infty}[-i(1-\frac{k_{ny}^2}{k_0^2})e^{ik_{ny}\Delta y/2}+i+R_H(\gamma_n) \\ \quad \cdot(1-\frac{k_{ny}^2}{k_0^2})\sin(k_{ny}\Delta y/2)e^{i2k_{ny}y_v}]\frac{1}{k_{nx}k_{ny}^2}\sin(k_{nx}\Delta x/2) \\ \qquad\qquad v=q\ u=p. \end{cases} \tag{26}$$

In (24) and (25) $\mathrm{sgn}(x)$ is the sign function defined by

$$\mathrm{sgn}(x) = \begin{cases} +1 & \text{if } x>0 \\ -1 & \text{if } x<0. \end{cases} \tag{27}$$

All series in (24), (25), and (26) are exponentially convergent and thus the series can be truncated for relatively small n. This is also the case for (23) except for one term in the summand of the expressions corresponding to $v=q$. The convergence rate of

$$S=\sum_{n=-\infty}^{+\infty} i\frac{(1-k_{nx}^2/k_0^2)}{k_{nx}k_{ny}^2}\cdot\sin(k_{nx}\Delta x/2)e^{-ik_{nx}(x_u-x_p)} \tag{28}$$

is very poor and in order to improve the convergence rate the standard trick is to add and subtract a series whose summand is asymptotic to the original series. For large n

$$k_{nx}\approx\frac{2\pi n}{L} \qquad k_{ny}\approx i\frac{2\pi n}{L}$$

and the summand is approximated by

$$\frac{i}{k_0^2}\frac{L}{2\pi n}\sin(k - nx\Delta x/2)e^{-ik_{nx}(x_u - x_p)}$$

where the asymptotic forms for k_{nx} and k_{ny} are only used in the amplitude factor. It can be shown that

$$\sum_{n=-\infty, n\neq 0}^{+\infty} \frac{e^{in\alpha}}{n} = i\mathrm{sgn}(\alpha)(\pi - \mid \alpha \mid) \tag{29}$$

where α is a real number. By employing (29), a closed form for the asymptotic series (S_{app}) can be obtained and is given by

$$S_{app} = \begin{cases} \frac{L}{2k_0^2}e^{-ik_{nx}(x_u - x_p)}[\mathrm{sgn}(x_p - x_u)(1 - \frac{2|x_p - x_u|}{L})\sin(k_0 \sin\phi_0 \Delta x/2) \\ \quad -\frac{i\Delta x}{L}\cos(k_0 \sin\phi_0 \Delta x/2)] & x_p \neq x_u \\ \frac{iL}{2k_0^2}(1 - \frac{\Delta x}{L})\cos(k_0 \sin\phi_0 \Delta x/2) & x_u = x_p \end{cases}$$

Now (28) can be written as

$$S = \frac{i}{k_0^2}\sum_{\substack{n=-\infty \\ n\neq 0}}^{+\infty}[\frac{k_0^2 - k_{nx}^2}{k_{nx}k_{ny}^2} - \frac{L}{2\pi n}]\sin(k_{nx}\Delta x/2)e^{-ik_{nx}(x_u - x_p)} + \frac{i\sin(k_0 \sin\phi_0 \Delta x/2)}{k_0^3 \sin\phi_0} + S_{app}$$

in which case the series converges very fast.

The right-hand-side of the matrix equations may be represented by an excitation vector whose elements, for E polarization, are

$$b(u,v) = ik_0 Y_0(\epsilon(x_u, y_v) - 1)e^{ik_0 \sin\phi_0 x_u}[e^{-ik_0 \cos\phi_0 y_v} + R_E(\phi_0)e^{ik_0 \cos\phi_0 y_v}]$$

The excitation vector for H polarization is made up of two sub-vectors with entries

$$b_1(u,v) = ik_0 Y_0(\epsilon(x_u, y_v) - 1)\cos\phi_0 e^{ik_0 \sin\phi_0 x_u}[-e^{-ik_0 \cos\phi_0 y_v} + R_H(\phi_0)e^{ik_0 \cos\phi_0 y_v}],$$

$$b_2(u,v) = -ik_0 Y_0(\epsilon(x_u, y_v) - 1)\sin\phi_0 e^{ik_0 \sin\phi_0 x_u}[e^{-ik_0 \cos\phi_0 y_v} + R_H(\phi_0)e^{ik_0 \cos\phi_0 y_v}].$$

We point out that the inhomogeneous layer may have an arbitrary thickness profile with a maximum height t. In such cases we may assume that the layer has a constant thickness t and the permittivity corresponding to air-filled points is 1.

3 High Frequency Scattering from Stratified Cylinders

For dielectric cylinders with large radii of curvature, physical optics may be used to obtain the scattered field provided the dielectric has sufficient loss to prevent significant penetration through the cylinder. The dielectric loss also suppresses the effects of creeping waves which enhances the physical optics results. If the dielectric cylinder is stratified, the physical optics approximation could still be used if the radius of curvature of all the interface contours are much larger than the wavelength.

Two types of physical optics approximations can be applied: 1) surface integral and 2) volume integral approximation . In surface integral physical optics the equivalent surface currents are approximated by electric and magnetic surface currents of the infinite tangential plane. In the latter method the volumetric polarization current is estimated by finding the internal field using geometrical optics ray tracing. Of the two techniques, the surface integral physical optics is much easier to employ. New physical optics surface currents [Sarabandi et al 1990] that are more convenient to use than the standard ones [Beckmann 1968] are examined. These currents can be obtained by noting that the reflected plane wave from

a dielectric interface can be generated by equivalent electric and magnetic current sheets. These currents are normal to the plane of incidence and their density is proportional to the incident field amplitude, polarization, and associated Fresnel reflection coefficient. Suppose the incident field is given by

$$\mathbf{E}^i = \mathbf{E}_0 e^{ik_0 \hat{k}_i \cdot \mathbf{r}} \quad , \qquad \mathbf{H}^i = \mathbf{H}_0 e^{ik_0 \hat{k}_i \cdot \mathbf{r}}$$

and the normal to the cylinder surface is represented by the unit vector $\hat{n}$. The unit vector normal to the plane of incidence is

$$\hat{t} = \frac{\hat{n} \times \hat{k}_i}{| \hat{n} \times \hat{k}_i |},$$

in terms of which the new physical optics electric and magnetic currents are given by

$$\mathbf{J}_e = -2Y_0(\mathbf{E}_0 \cdot \hat{t}) \cos\phi_i R_E(\phi_i) e^{ik_0 \hat{k}_i \cdot \mathbf{r}} \hat{t} \tag{30}$$

$$\mathbf{J}_m = -2Z_0(\mathbf{H}_0 \cdot \hat{t}) \cos\phi_i R_H(\phi_i) e^{ik_0 \hat{k}_i \cdot \mathbf{r}} \hat{t} \tag{31}$$

Here, R_E and R_H are Fresnel reflection coefficients and ϕ_i is the local angle of incidence given by

$$\phi_i = \arccos(-\hat{n} \cdot \hat{k}_i).$$

In shadow regions on the surface ($\phi_i > \pi/2$) the currents are zero.

Suppose a stratified cylinder with arbitrary cross section is illuminated by a plane wave travelling in $-x$ direction ($\hat{k}_i = -\hat{x}$) as shown in Fig. 4. The outer

surface of the cylinder is described by a smooth function $\rho(\phi)$. For E-polarized wave ($\mathbf{E}_0 = \hat{z}$) only electric current and for H-polarized wave ($\mathbf{H}_0 = Y_0\hat{z}$) only magnetic current is induced on the cylinder surface as given by (30) and (31). It can easily be shown that in the far zone of the cylinder in a direction denoted by ϕ_s, the far field amplitudes for E and H polarization respectively are given by

$$\mathbf{S}_E = \hat{z}\frac{k_0}{2}\int_{\text{lit}} \cos\phi_i R_E(\phi_i) e^{-ik_0\rho(\phi')(\cos\phi' + \cos(\phi' - \phi_s))}\sqrt{\rho^2(\phi') + \rho'^2(\phi')}\,\mathrm{d}\phi' \qquad (32)$$

$$\mathbf{S}_H = \hat{\phi}\frac{k_0}{2}\int_{\text{lit}} \cos\phi_i R_H(\phi_i) e^{-ik_0\rho(\phi')(\cos\phi' + \cos(\phi' - \phi_s))}\sqrt{\rho^2(\phi') + \rho'^2(\phi')}\,\mathrm{d}\phi' \qquad (33)$$

where the integral is taken over the lit region and ρ' is the derivative of ρ with respect to ϕ. If the surface of the cylinder is convex the integral in (32) and (33)

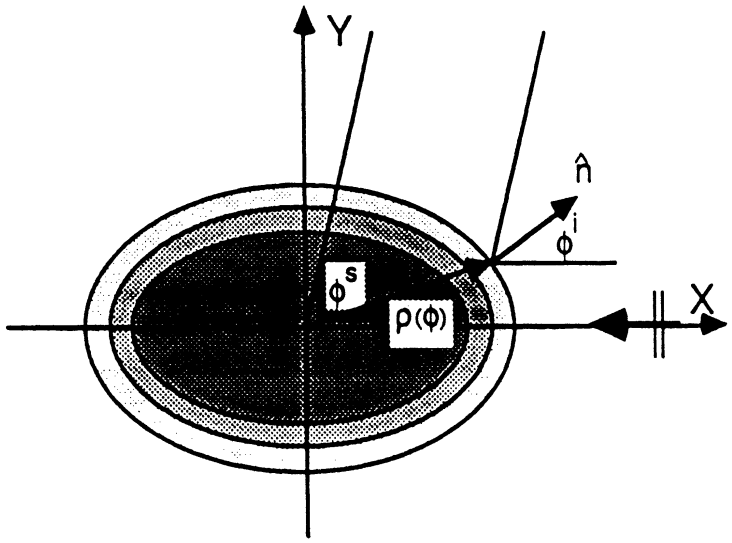

Figure 4: Geometry of scattering problem of a stratified cylinder.

can be evaluated using the stationary phase technique. The stationary point (ϕ_{SP})

is the root of the equation

$$\frac{\mathrm{d}}{\mathrm{d}\phi'}\rho(\phi')\left(\cos\phi' + \cos(\phi' - \phi_s)\right) = 0.$$

By noting that at the stationary point $\phi_i = \phi_s/2$ and

$$\sqrt{\rho^2(\phi') + \rho'^2(\phi')} = \frac{\rho(\phi_{SP})}{\cos(\phi_{SP} - \phi_s/2)},$$

and also by defining

$$g = \frac{\mathrm{d}^2}{\mathrm{d}\phi'^2}[\rho(\phi')\left(\cos\phi' + \cos(\phi' - \phi_s)\right)]_{\phi'=\phi_{SP}}$$

equations (32) and (33) become

$$\mathbf{S}_E = \hat{z}\cos(\frac{\phi_s}{2})R_E(\frac{\phi_s}{2})\frac{\rho(\phi_{SP})}{\cos(\phi_{SP} - \phi_s/2)}\sqrt{\frac{k_0\pi}{2\mid g\mid}}$$
$$\cdot e^{-ik_0\rho(\phi_{SP})(\cos\phi_{SP} + \cos(\phi_{SP} - \phi_s))} \cdot e^{-i\mathrm{sgn}(g)\frac{\pi}{4}}, \tag{34}$$

$$\mathbf{S}_H = \hat{\phi}\cos(\frac{\phi_s}{2})R_H(\frac{\phi_s}{2})\frac{\rho(\phi_{SP})}{\cos(\phi_{SP} - \phi_s/2)}\sqrt{\frac{k_0\pi}{2\mid g\mid}}$$
$$\cdot e^{-ik_0\rho(\phi_{SP})(\cos\phi_{SP} + \cos(\phi_{SP} - \phi_s))} \cdot e^{-i\mathrm{sgn}(g)\frac{\pi}{4}}. \tag{35}$$

For a circular cylinder of radius a these expressions simplify to

$$\mathbf{S}_E = \hat{z}\frac{1}{2}\sqrt{k_0\pi a\cos(\phi_s/2)}R_E(\frac{\phi_s}{2})e^{-i2k_0 a\cos(\phi_s/2)}e^{i\pi/4} \tag{36}$$

$$\mathbf{S}_H = \hat{\phi}\frac{1}{2}\sqrt{k_0\pi a\cos(\phi_s/2)a}R_H(\frac{\phi_s}{2})e^{-i2k_0 a\cos(\phi_s/2)}e^{i\pi/4} \tag{37}$$

To verify the validity of the physical optics expressions with new set of physical optics currents we compare expressions (37) and (38) for a layered circular cylinder

with the exact series solution [Ruck et al, 1970, pp. 259]. Let us consider a two-layer cylinder with inner and outer radii of $a_1 = 10cm$ and $a = 10.5cm$ respectively. The dielectric constant of the inner and outer layers respectively are $15+i7$ and $4+i1$. These values are so chosen to simulate a tree with smooth bark. Figures 5 and 6 compare the normalized backscattering cross section ($\sigma/\pi a$) of the cylinder for E and H polarizations using physical optics expressions and exact series solution. In these figures the cross section of the cylinder in absence of the outer layer (bark) is also plotted to demonstrate the effect of the bark on reducing the cross section of the cylinder. For frequencies above 2 GHz ($k_0 a = 4.2$) the agreement between the two solution is excellent. The bark layer plays the role of an impedance transformer which reduces the cross section of the cylinder by 14 dB around $k_0 a = 16$.

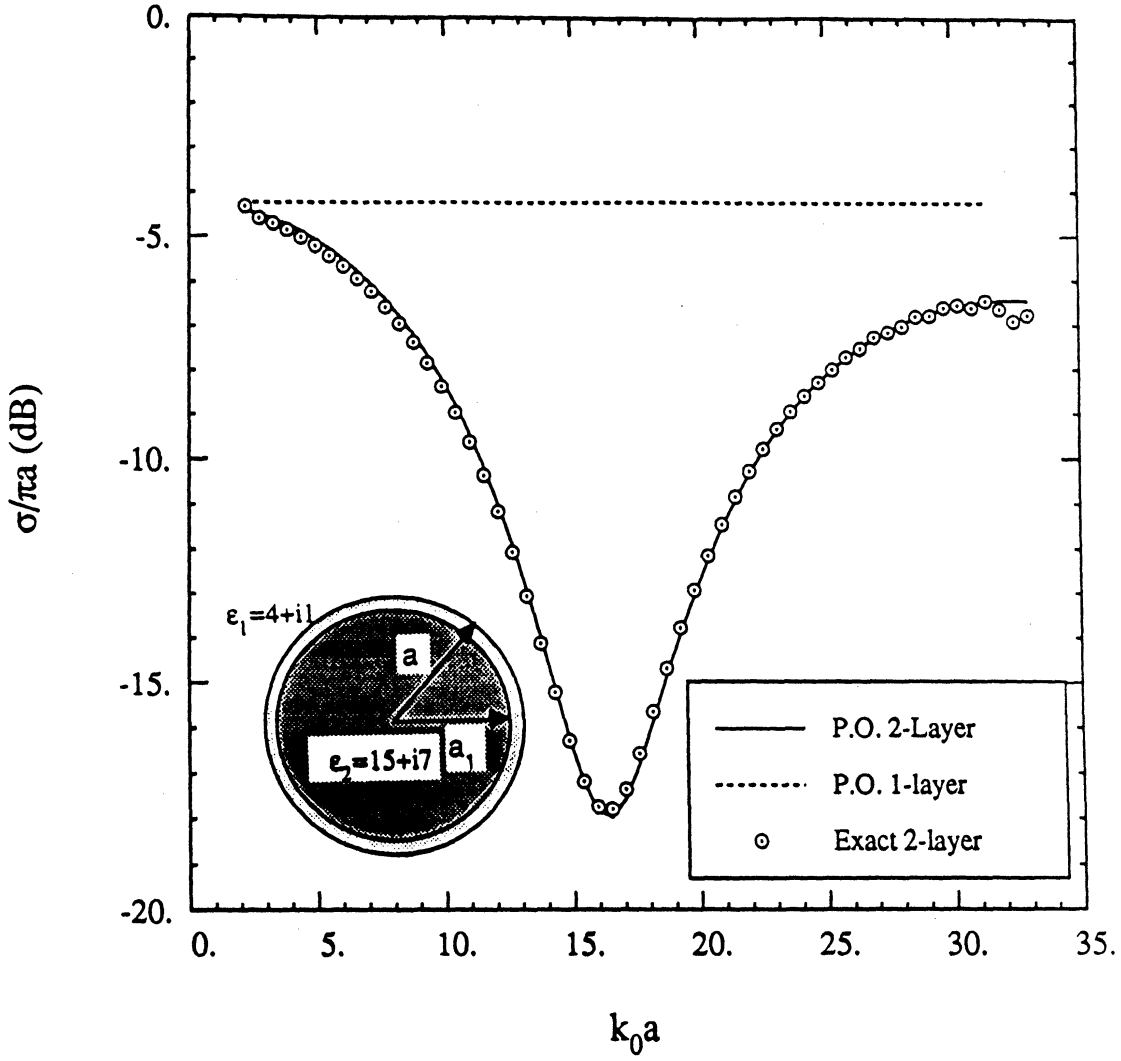

Figure 5: Normalized backscattering cross section ($\frac{\sigma}{\pi a}$) of a two-layer dielectric cylinder with $a = 10.5cm$, $a_1 = 10cm$, $\epsilon_1 = 15 + i7$, $\epsilon_2 = 4 + i1$ versus $k_0 a$ for TM case.

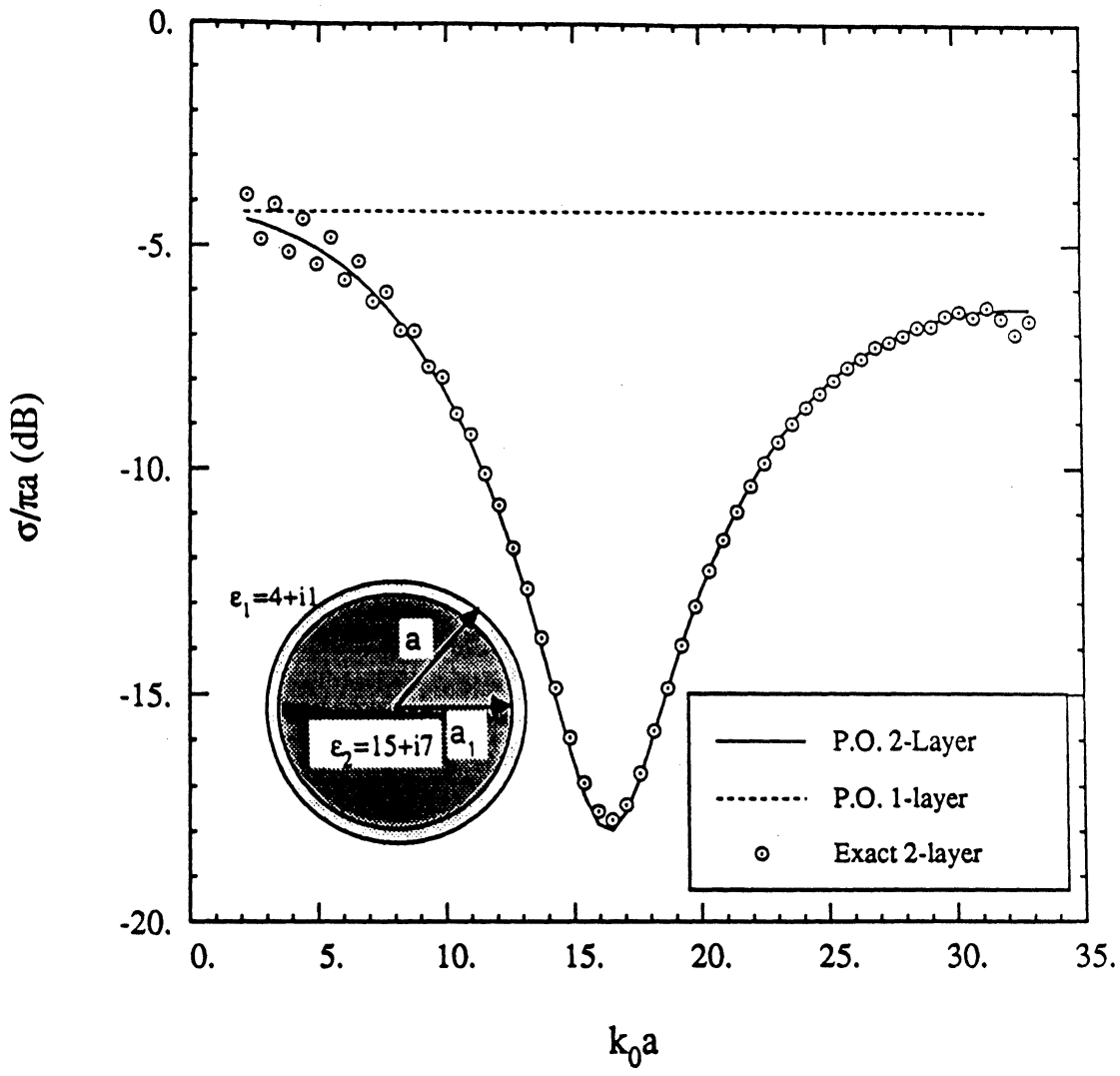

Figure 6: Normalized backscattering cross section ($\frac{\sigma}{\pi a}$) of a two-layer dielectric cylinder with $a = 10.5cm$, $a_1 = 10cm$, $\epsilon_1 = 15 + i7$, $\epsilon_2 = 4 + i1$ versus $k_0 a$ for TE case.

4 Scattering from Corrugated Cylinder

Consider a corrugated dielectric cylinder with arbitrary cross section as shown in Fig. 7. Assume the corrugation geometry is such that the humps are identical and of equal distance L from each other. Further assume that if the corrugation is removed the surface of the cylinder would be denoted as before by $\rho(\phi)$ and the radius of curvature at each point is much larger than the wavelength and L. Under

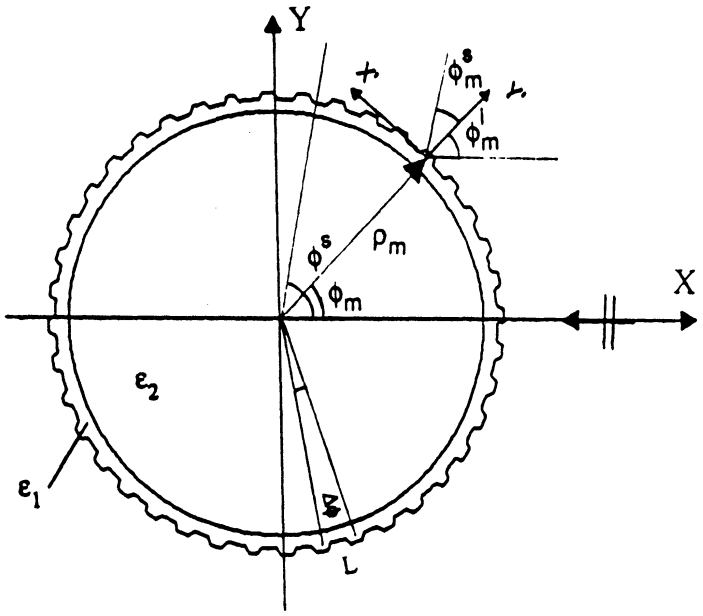

Figure 7: A corrugated cylinder geometry.

these conditions each point on the cylinder surface can be replaced, approximately, by a periodic corrugated surface. The accuracy of this approximation is in the order of physical optics approximation for smooth cylinders.

Suppose the cylinder is illuminated by a plane wave travelling in $-x$ direction and let us denote the tangential coordinate at the center of each hump by (x', y') where $\hat{y'}$ coincides with the outward normal unit vector $(\hat{n}(\phi))$. If the origin of the

prime coordinate system corresponding to the m^{th} hump is located at (ρ_m, ϕ_m) we have

$$\phi_m = \sum_{\ell=1}^{m} \Delta\phi_\ell - \frac{\pi}{2}, \tag{38}$$

$$\Delta\phi_{\ell+1} = \frac{L}{\sqrt{\rho^2(\phi_\ell) + \rho'^2(\phi_\ell)}}, \tag{39}$$

where $\Delta\phi_1$ is a known quantity. The local incidence angle at the m^{th} hump can be obtained from

$$\phi_m^i = \arccos(\hat{n}(\phi_m) \cdot \hat{x})$$

and the induced current in the m^{th} hump can be approximated by that of the periodic corrugated surface when the incidence angle is ϕ_m^i. The scattering direction is denoted by ϕ_s as before and the scattering direction for the m^{th} local coordinate is given by

$$\phi_m^s = \phi_s - \phi_m^i.$$

The far field due to the m^{th} hump ($\mathbf{S}_m$), depending on the polarization, can be obtained from (10) and we note that those humps with $| \phi_m^s | > \pi/2$ do not contribute to the far field. The total contribution of the cylinder corrugation to the far field is the vector sum of the fields due to each hump modified by a phase factor to correct for the relative positions of the humps. Therefore

$$\mathbf{S}_c = \sum_m \mathbf{S}_m e^{-ik_0 x_m} e^{-ik_0(x_m \cos\phi_s + y_m \sin\phi_s)}, \tag{40}$$

where

$$x_m = \rho_m \cos \phi_m,$$

$$y_m = \rho_m \sin \phi_m.$$

The total scattered field may now be obtained from

$$\mathbf{S} = \mathbf{S}_c + \mathbf{S}_s,$$

where $\mathbf{S}_s$ is the far field amplitude of the smooth cylinder.

5 Numerical Results

To examine the effect of surface corrugation on scattering from corrugated cylinders, we consider a two-layer circular cylinder with uniform corrugation. The pertinent parameters are chosen as follows: each hump is a $\lambda_0/8 \times \lambda_0/8$ square with dielectric constant $\epsilon_1 = 4 + i1$, the distance between humps is $L = \lambda_0/4$, the thickness and dielectric constant of outer layer are $\lambda_0/2$ and $4 + i1$ respectively, and the radius and the dielectric constant of inner layer are $10\lambda_0$ and $15 + i7$ respectively. For the corresponding periodic surface (see Fig. 8) all the components of the induced current in each hump are obtained by the moment method and the amplitude and phase of the total current ($\int_s J(x', y')\mathrm{d}x'\mathrm{d}y'$) are plotted in Figs. 9 and 10. Figures 11-14 show the amplitude and the phase of the zeroth Bragg mode as given in (20) and (21), the reflected wave in the absence of the corrugations, and the sum of the two waves (total reflected wave) as a function of incidence angle. For E polarization (Fig. 11) the total reflected wave is less than the reflected wave

in the absence of corrugation (reduction in the scattered field). In this case, as far as the total reflected field is concerned, the corrugation can be replaced by a homogeneous dielectric layer with thickness $\lambda_0/8$ and $\epsilon = 2.6 + i0.58$. For H polarization (Fig. 13) the total reflected wave is weaker than the reflected wave in the absence of the corrugation for angles less than the Brewster angle and vice versa for angles greater than the Brewster angle.

Once the induced current versus angle is obtained the bistatic scattered field can be computed from (41). Figures 14 and 15 show the radar cross section due to the corrugation (σ_c) and smooth cylinder (σ_s) and the total radar cross section ($\sigma_c + \sigma_s$). To examine the role of the outer layer, the radar cross section of the cylinder (1-layer) when the outer layer is removed is also plotted. It is seen that the smooth bark reduces the scattered field by 3 dB and the corrugation on the bark further reduces the scattered field by another 8 dB. In Fig. 16 the radar cross section of the corrugated cylinder, for both polarizations, are compared with a smooth cylinder when corrugation is replaced by an equivalent uniaxial dielectric layer as explained in Appendix A. The thickness and dielectric tensor elements respectively are $t = \lambda_0/8$, $\epsilon_y = \epsilon_z = 2.6 + i0.58$, and $\epsilon_x = 1.81 + i0.78$. Excellent agreement is obtained.

6 Conclusions

A hybrid solution based on the moment method and physical optics approximation is obtained for corrugated layered cylinders. The only restriction on the physical

dimensions is the radius of curvature (r) of the cylinder where we require $r \gg \lambda_0$. Also new physical optics expressions for the equivalent surface current on the dielectric structure is introduced. Also it is shown that when period of the corrugation is smaller than the half a wavelength the corrugation can be modeled by an uniaxial dielectric layer which extremely simplifies the problem.

This method is employed to investigate the effect of bark and its roughness on the scattering from tree trunks and branches. It is shown that the bark and its roughness both reduce the radar cross section. The low contrast dielectric bark layer manifest its effect more significantly at higher frequencies where the bark thickness and its roughness are a considerable fraction of the wavelength.

Acknowledgement

This work was supported by the NASA under contract NAGW-1101.

References

[1] Beckmann, P., The Depolarization of Electromagnetic Waves, Boulder, Co: The Golem Press, 1968.

[2] Bodnar, D.G, and H.L. Bassett, "Analysis of an anisotropic dielectric Radome," *IEEE Trans. Antennas Propag.*, pp. 841-846, Nov. 1975.

[3] Cabayan, H.S., and R.C. Murphy, "Scattering of electromagnetic waves by rough perfectly conducting circular cylinders," *IEEE Trans. Antennas Propag.*, 21, pp. 893-895, 1973.

[4] Clemmow, P.C., and V.H. Weston, "Studies in radar cross section XXXVI-Diffraction of a plane wave by an almost circular cylinder," *Radiation Laboratory Report No. 2871-3-T*, The University of Michigan, Sept. 1959.

[5] Karam, M.A., and A.K. Fung, "Electromagnetic scattering from a layer of finite length, randomly oriented, dielectric, circular cylinders over a rough interface with application to vegetation," *International Journal of Remote Sensing*, 9, pp. 1109-1134, 1988.

[6] Kong ,J.A., Electromagnetic Wave Theory, New York: John Wiley & Sons, 1985.

[7] Morita, T., and S.B. Cohen, "Microwave lense matching by simulated quarter-wave transformers," *IRE Trans. Antennas Propag.*, pp.33-39, Jan. 1956.

[8] Padman, R. "Reflection and cross-polarization properties of grooved dielectric panels," *IEEE Trans. Antennas Propag.*, 26, pp. 741-743, 1978.

[9] Sarabandi, K., F.T. Ulaby, and T.B.A. Senior, "Millimeter wave scattering model for a leaf", *Radio Sci.*, accepted for publication.

[10] Tong, T.C., "Scattering by a slightly rough cylinder and a cylinder with impedance boundary condition," *Int. J. Electron.*, 36, pp. 767-772, 1974.

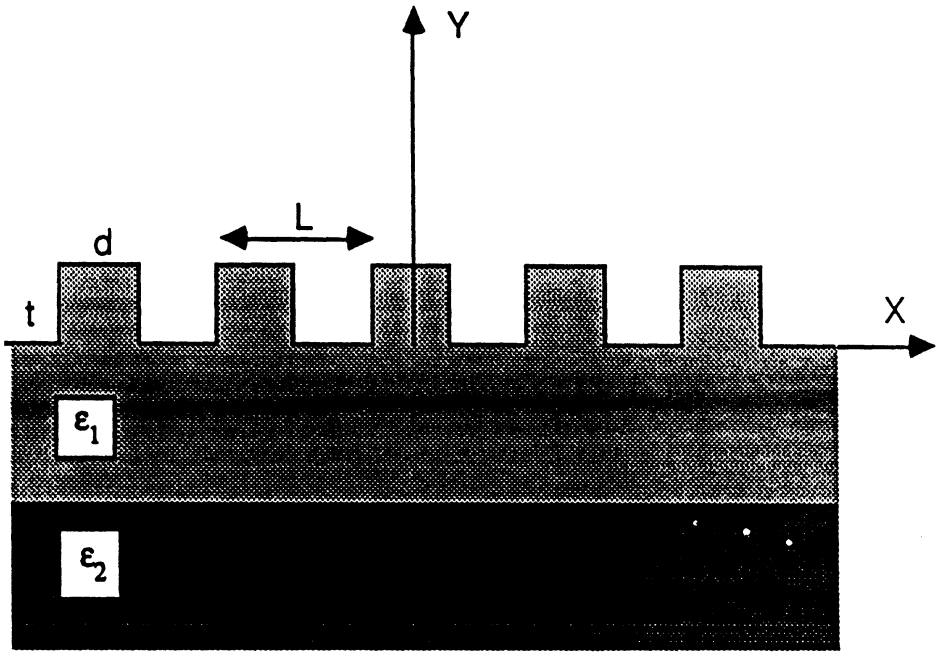

Figure 8: Geometry of the corrugated surface

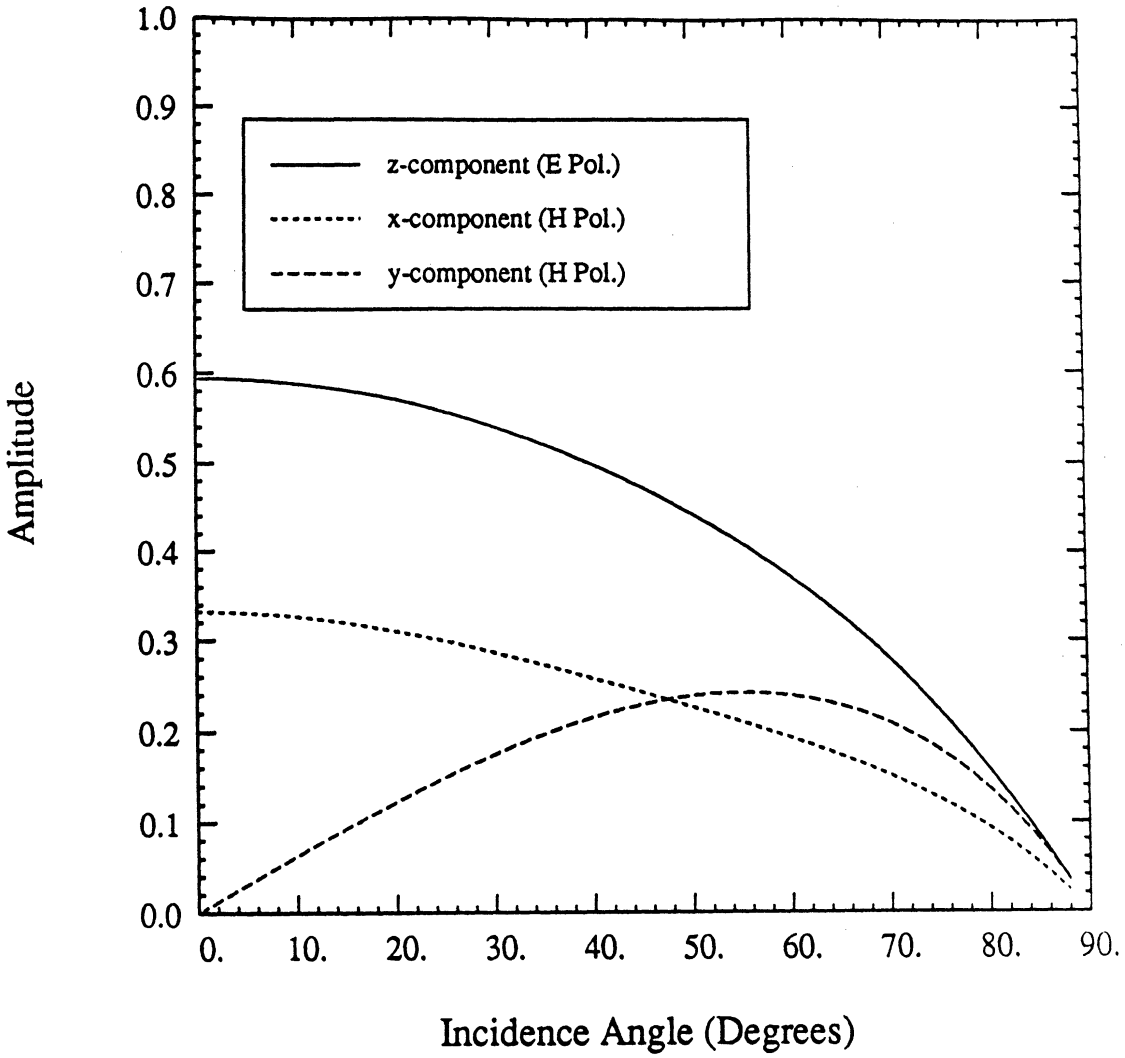

Figure 9: Amplitude of the total induced current in the two-layer periodic corrugated surface versus incidence angle.

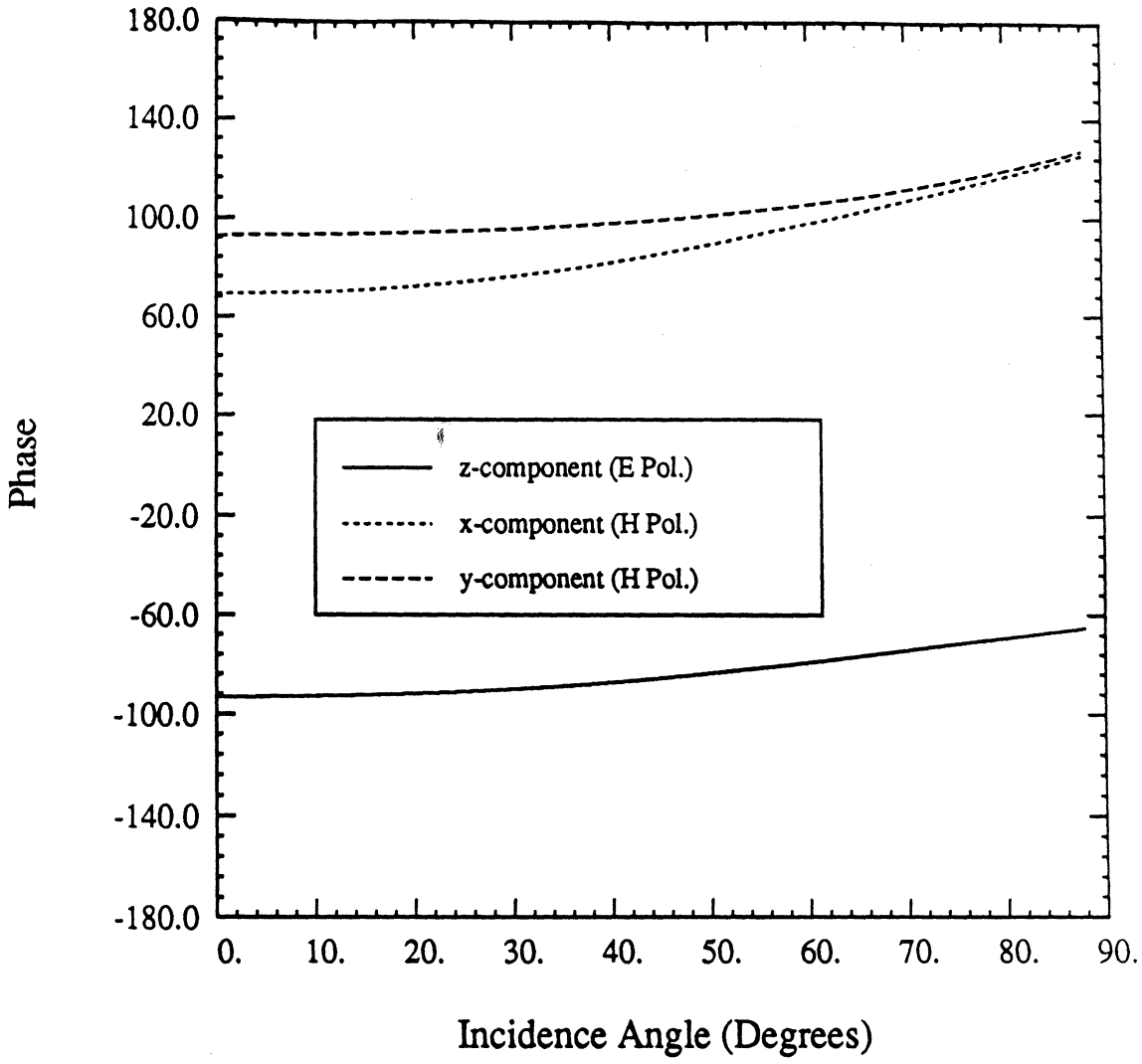

Figure 10: Phase of the total induced current in the two-layer periodic corrugated surface versus incidence angle.

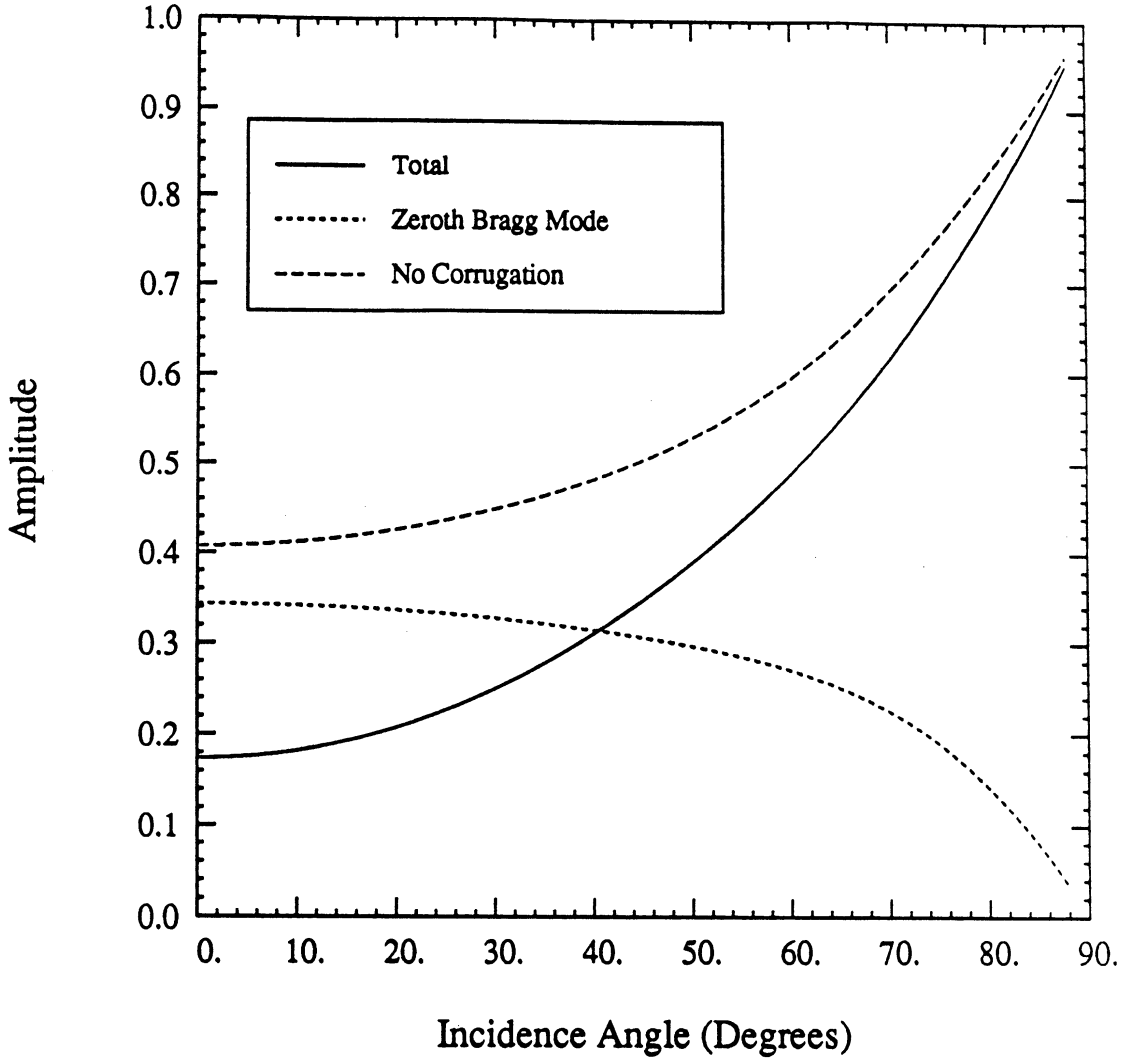

Figure 11: Amplitude of the reflected field from the two-layer periodic corrugated surface versus incidence angle for E polarization.

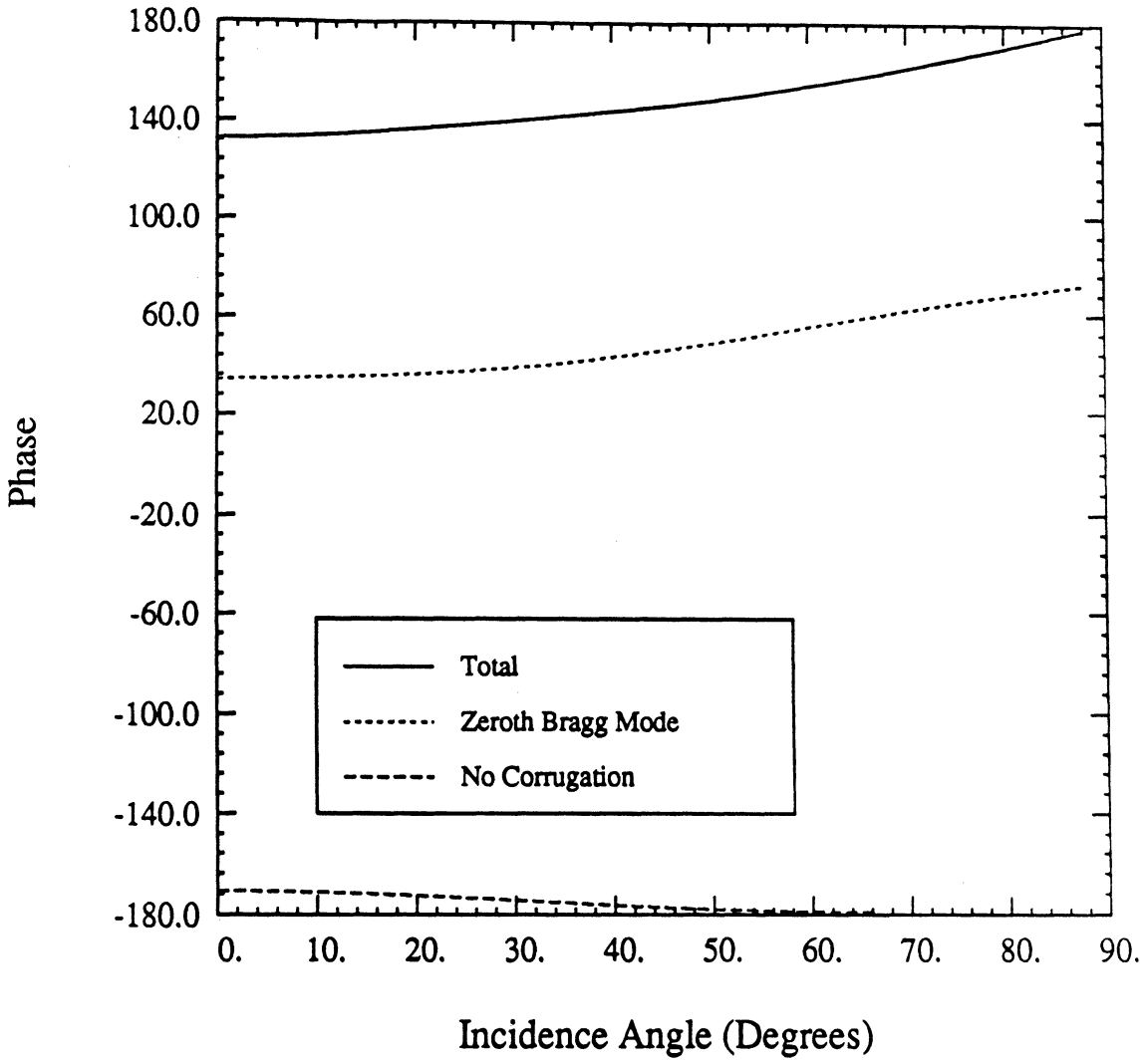

Figure 12: Phase of the reflected field from the two-layer periodic corrugated surface versus incidence angle for E polarization.

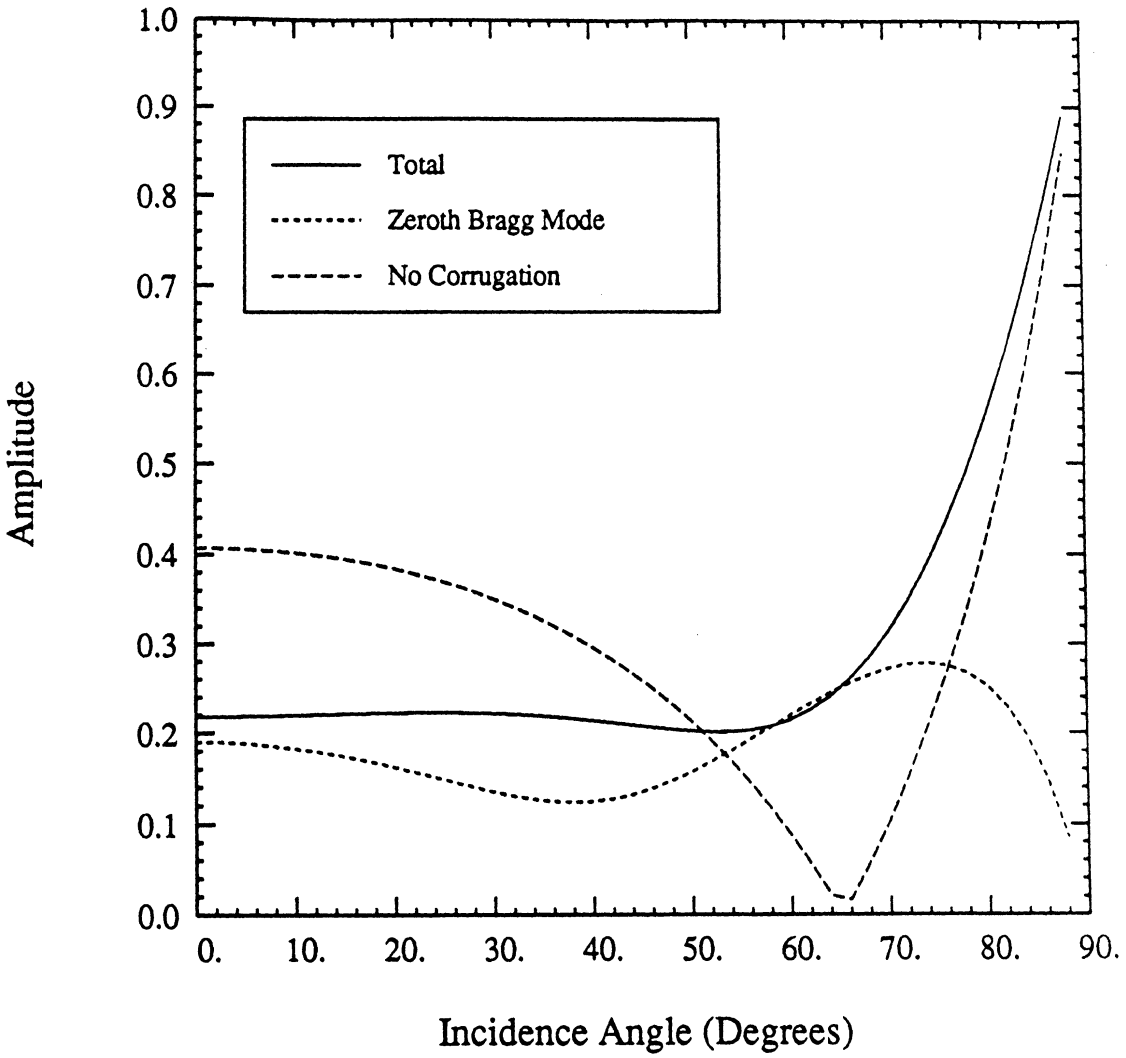

Figure 13: Amplitude of the reflected field from the two-layer periodic corrugated surface versus incidence angle for H polarization.

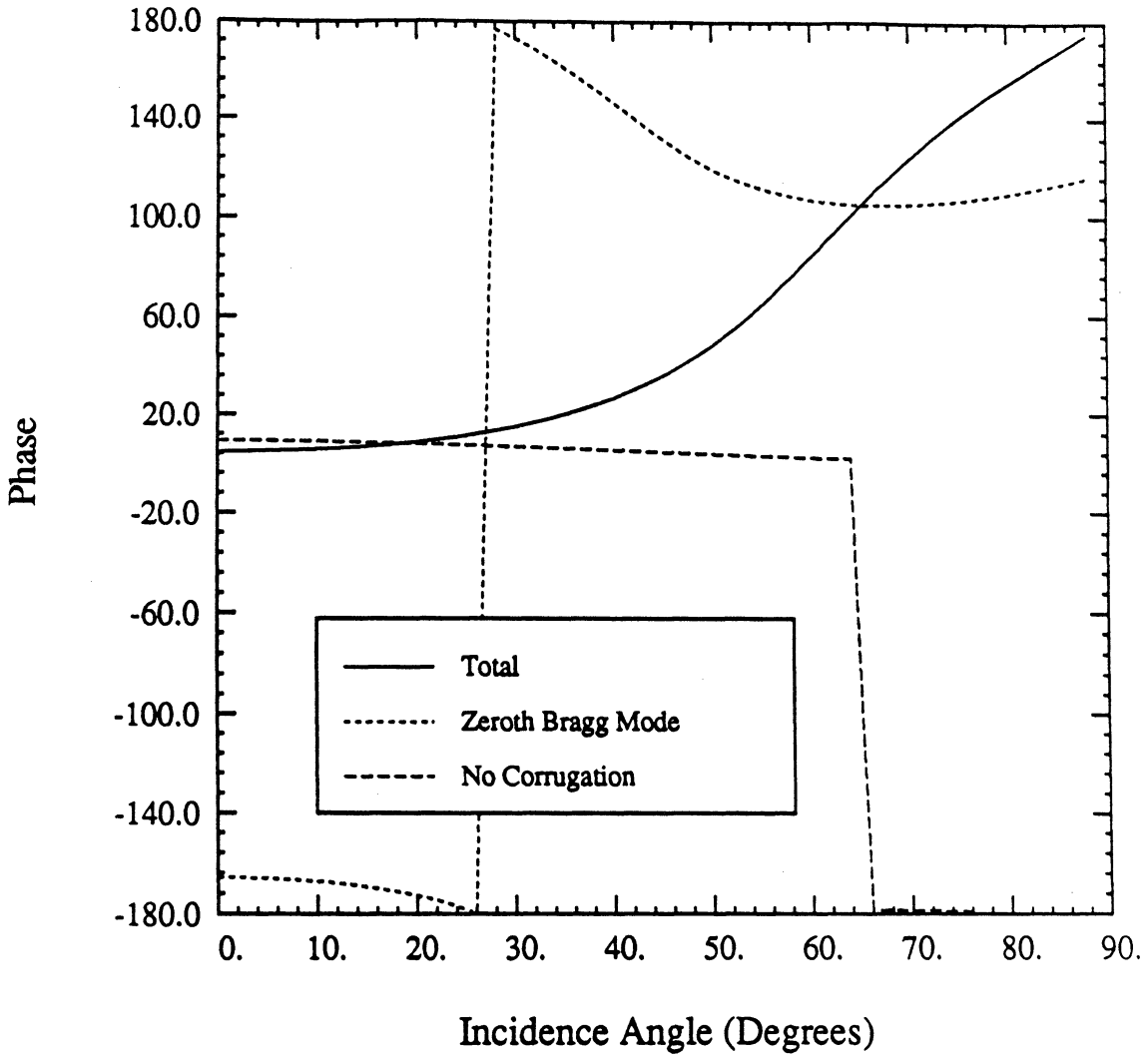

Figure 14: Phase of the reflected field from the two-layer periodic corrugated surface versus incidence angle for H polarization.

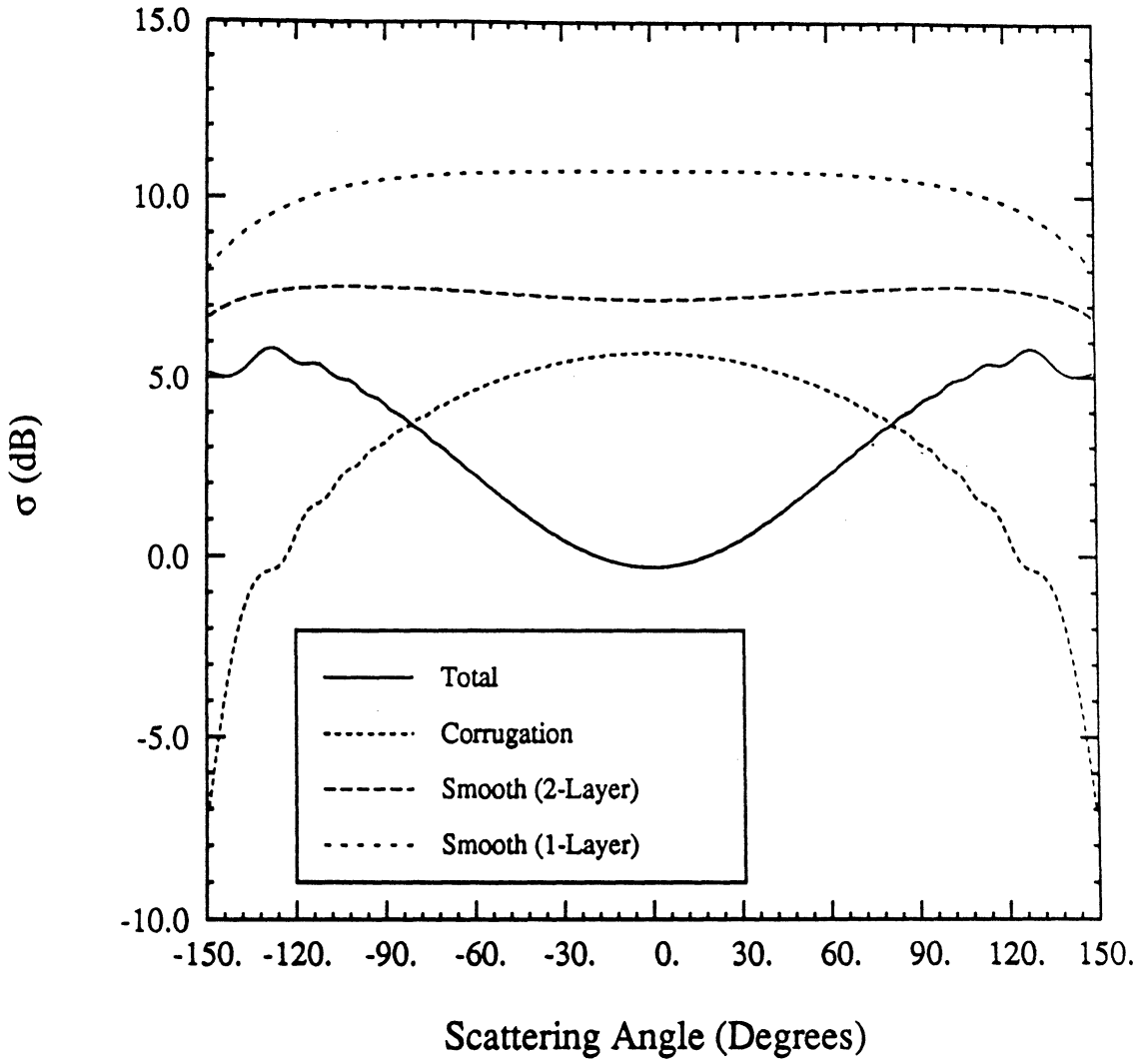

Figure 15: The radar cross section of a corrugated cylinder for TM case with $a = 10.5\lambda_0$, $a_1 = 10\lambda_0$, $L = \lambda_0/4$, $\epsilon_1 = 4 + i1$, $\epsilon_2 = 15 + i7$, and $t = d = \lambda_0/8$.

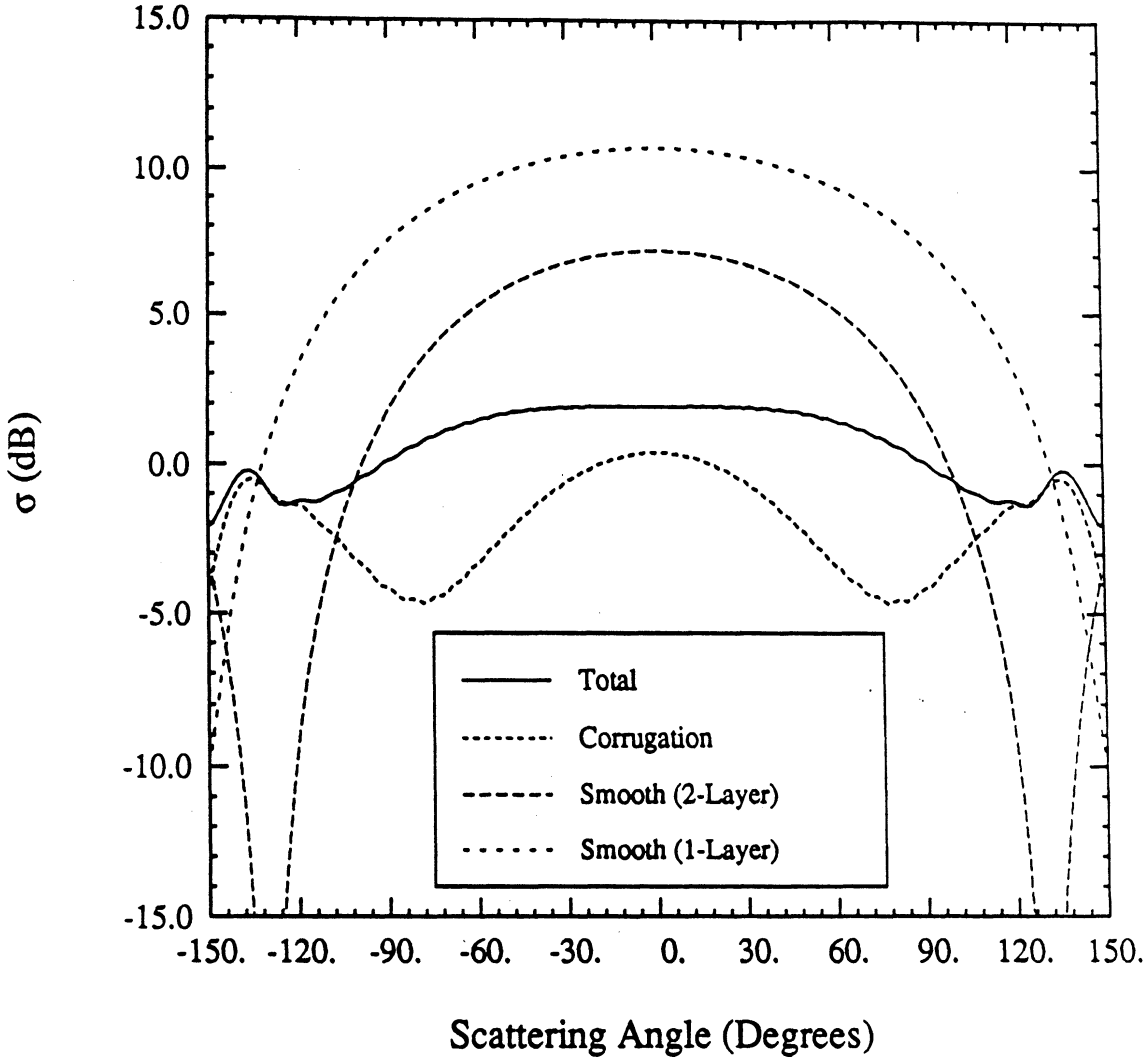

Figure 16: The radar cross section of a corrugated cylinder for TE case with $a = 10.5\lambda_0$, $a_1 = 10\lambda_0$, $L = \lambda_0/4$, $\epsilon_1 = 4 + i1$, $\epsilon_2 = 15 + i7$, and $t = d = \lambda_0/8$.

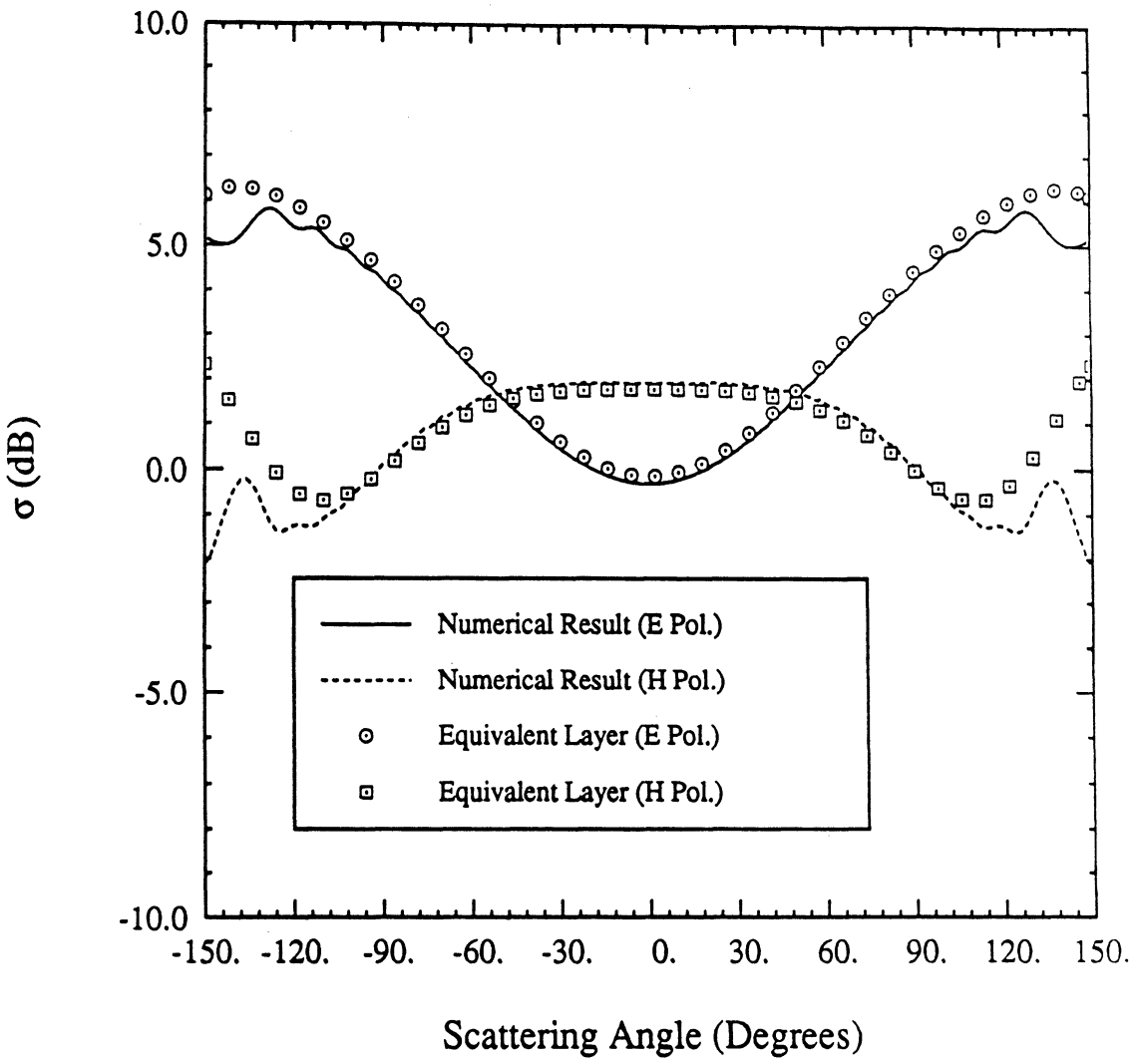

Figure 17: The radar cross section of the corrugated cylinder for TE and TM cases using the numerical and the equivalent dielectric methods.

APPENDIX A
SIMULATION OF AN ARRAY OF DIELECTRIC SLABS WITH AN EQUIVALENT ANISOTROPIC MEDIUM

A1 Introduction

Our purpose in this appendix is to find the equivalent dielectric constant of a medium comprised of homogeneous dielectric slabs of identical material which are equally spaced. Depending on the polarization of the fields and the boundary conditions imposed, a variety of different modes can be supported by this structure. Modeling of grooved-dielectric surfaces with anisotropic homogeneous media, to our knowledge, was first studied by Morita and Cohen. They analyzed this problem by simulating the infinite periodic array using a partially-filled waveguide, then, by solving the appropriate transcedental equation the propagation constant in the corrugation was obtained. These results are used in many problems such as matching dielectric lens surfaces [Morita and Cohen, 1956] and designing broadband radomes [Bodnar and Bassett, 1975; Padman, 1978].

Since the interest is in the modes that are excited by an incident plane wave, simulating the array by a partially-filled waveguide which forces the tangential electric field to be zero at the waveguide walls may not be appropriate. Here we impose a condition that supports the modes which would be excited by a plane wave incident on the structure. This approach will provide a formula for the elements of the equivalent dielectric tensor which is different from that reported by Morita and Cohen. The validity of this technique is verified by numerical solution

of corrugated surfaces in Section A5. In Section A4 the reflection coefficient of uniaxial layered media is derived to extend the applicabilities of the equivalent dielectric technique to periodic surfaces with arbitrary cross sections.

A2 Theoretical Analysis

To proceed with the analysis, suppose that similar dielectric slabs of an infinite array with thickness d and dielectric constant ϵ are parallel to the y-z plane. Further assume that the period of the structure is denoted by L. The geometry of the problem is depicted in Fig. A-1. If the x-y plane is the plane of incidence, the solution is independent of z and therefore the waves can be separated into E- and H-polarized waves. Each period of the medium can be divided into two regions

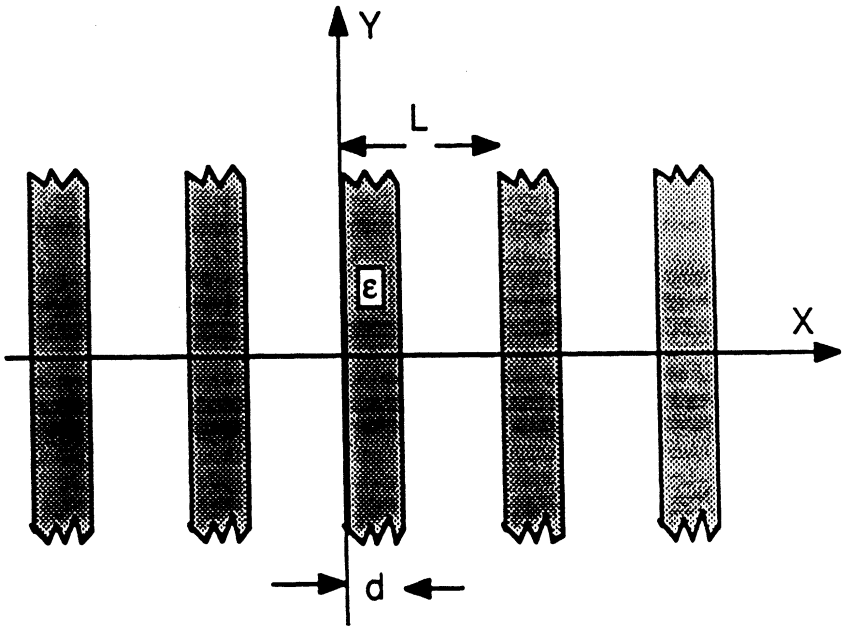

Figure A-1: An array of infinite dielectric slabs.

and, depending on the polarization, the z component of the electric or magnetic

field must satisfy the wave equation, i.e.

$$\left(\frac{\partial^2}{\partial x^2}+\frac{\partial^2}{\partial y^2}+\epsilon k_0^2\right)\Psi^I(x,y)=0 \qquad 0\le x\le d \tag{A1}$$

$$\left(\frac{\partial^2}{\partial x^2}+\frac{\partial^2}{\partial y^2}+k_0^2\right)\Psi^{II}(x,y)=0 \qquad d\le x\le L \tag{A2}$$

where $\Psi(x,y)=E_y(x,y)$ or $H_y(x,y)$. Using separation of variables and requiring the phase matching condition, the solutions of (A1) and (A2) take the following forms

$$\Psi^I(x,y)=\left[Ae^{ik_x^I x}+Be^{-ik_x^I x}\right]e^{ik_y y} \tag{A3}$$

$$\Psi^{II}(x,y)=\left[Ce^{ik_x^{II} x}+De^{-ik_x^{II} x}\right]e^{ik_y} \tag{A4}$$

where k_y is the propagation constant in the periodic medium which must satisfy

$$(k_x^I)^2+k_y^2=\epsilon k_0^2 \tag{A5}$$

$$(k_x^{II})^2+k_y^2=k_0^2 \tag{A6}$$

In an attempt to find the unknown coefficients, we notice that the tangential components of the electric and magnetic fields must be continuous at $x=d$ which constitutes two equations. Two more equations can be obtained by applying Floquet's theorem for periodic differential equations which requires $\Psi(x+L,y)=\sigma\Psi(x,y)$ for some constant σ. To set an appropriate value for σ suppose the medium is simulated with an equivalent homogeneous dielectric. If a plane wave illuminates the half-space of the equivalent homogeneous medium at an angle ϕ_0, the x dependency would be of the form $e^{ik_0\sin\phi_0 x}$. This dependency suggests that we need to

impose a progressive phase condition, i.e. let $\sigma = e^{ik_0 \sin\phi_0 L}$. Therefore the other two equations become

$$E_{\tan}(0+L,y) = e^{ik_0 \sin\phi_0 L} E_{\tan}(0,y) \tag{A7}$$

$$H_{\tan}(0+L,y) = e^{ik_0 \sin\phi_0 L} H_{\tan}(0,y) \quad . \tag{A8}$$

Application of the mentioned boundary conditions for the E polarization gives the following equations

$$\begin{aligned}
&Ae^{ik_x^I d} + Be^{-ik_x^I d} = Ce^{ik_x^{II} d} + De^{-ik_x^{II} d} \\
&k_x^I \left[Ae^{ik_x^I d} - Be^{-ik_x^I d}\right] = k_x^{II} \left[Ce^{ik_x^{II} d} - De^{-ik_x^{II} d}\right] \\
&A + B = \left[Ce^{ik_x^{II} l} + De^{-ik_x^{II} l}\right] e^{-ik_0 \sin\phi_0 L} \\
&k_x^I \left[A - B\right] = k_x^{II} \left[Ce^{ik_x^{II} l} - De^{-ik_x^{II} l}\right] e^{-ik_0 \sin\phi_0 L}
\end{aligned} \tag{A9}$$

Since we are interested in the nontrivial solution of the above linear equations the determinant of the coefficient matrix must be set to zero. This condition provides an equation for k_x^I and k_x^{II} and is given by

$$\begin{aligned}
-\left(\tfrac{k_x^I}{k_x^{II}} + \tfrac{k_x^{II}}{k_x^I}\right) \sin(k_x^I d) \sin\left(k_x^{II}(L-d)\right) + 2\cos(k_x^I d)\cos\left(k_x^{II}(L-d)\right) = \\
2\cos(k_0 \sin\phi_0 L)
\end{aligned} \tag{A10}$$

Dispersion relations (A5) and (A6) give rise to another equation for k_x^I and k_x^{II}, i.e.

$$(k_x^I)^2 - (k_x^{II})^2 = k_0^2(\epsilon - 1) \tag{A11}$$

The transcedental equation (A10) together with (A11) can be solved simultaneously to find the propagation constants. It is worth noting that in a limiting case

when the periodic medium approaches a homogeneous one then $k_x^I \rightarrow k_x^{II}$ and (A10) reduces to

$$\cos(k_x L) = \cos(k_0 \sin\phi_0 L)$$

which implies $k_x = k_0 \sin\phi_0$ as expected.

After solving (A10) and (A11) for k_x^{II}, the propagation constant in the y-direction can be obtained from

$$k_y^2 = k_0^2 - (k_x^{II})^2 \tag{A12}$$

It should be pointed out that the solution for k_x^{II} is not unique and therefore this structure can support many modes corresponding to different values of k_x^{II}. The dominant mode for this structure corresponds to a value of k_x^{II} such that the imaginary part of k_y is minimum. For the equivalent homogeneous medium with permittivity ϵ_z, the propagation constant in the y-direction would be

$$k_y^2 = k_0^2 \left(\epsilon_z - \sin^2\phi_0\right) \tag{A13}$$

Comparing (A12) and (A13) it can be deduced that

$$\epsilon_z = \sin^2\phi_0 + 1 - \left(\frac{k_x^{II}}{k_0}\right)^2 \tag{A14}$$

From the symmetry of the problem it is obvious that if the electric field is in the y-direction the equivalent dielectric would be the same, that is $\epsilon_y = \epsilon_z$.

Using a similar procedure the following transcedental equation for H polarization can be obtained

$$-\left(\frac{\epsilon k_x^{II}}{k_x^I} + \frac{k_x^I}{\epsilon k_x^{II}}\right)\sin(k_x^I d)\sin\left(k_x^{II}(L-d)\right) + 2\cos(k_x^I d)\cos\left(k_x^{II}(L-d)\right) = 2\cos(k_0 \sin\phi_0 L) \tag{A15}$$

The equivalent dielectric constant ϵ_x can be obtained from (A14) where k_x^{II} is the solution of (A15) and (A11). Since $\epsilon_x \neq \epsilon_y = \epsilon_z$ the equivalent medium is uniaxial with the optical axis being parallel to the x-axis.

A3 Low Frequency Approximation

An analytical solution of equations (A10) and (A15) for k_x^I and k_x^{II} cannot be derived, in general, but using Newton's or Muller's method numerical solutions can easily be obtained. One of the cases where approximate expressions for ϵ_x and $\epsilon_y = \epsilon_z$ can be derived is the low frequency regime where $L < 0.2\lambda_0$. In this approximation the sine and cosine functions are replaced with their Taylor series expansion keeping up to the quadratic terms. Therefore equations (A10) and (A15), respectively, reduce to

$$\begin{cases} (k_x^I)^2 d + (k_x^{II})^2 (L-d) = (k_0 \sin\phi_0)^2 L \\ (k_x^I)^2 \frac{d}{\epsilon} + (k_x^{II})^2 (L-d) = (k_0 \sin\phi_0)^2 \frac{L^2}{\epsilon d + (L-d)} \end{cases} \tag{A16}$$

These equations together with (A11) can be solved easily to obtain

$$\epsilon_y = \epsilon_z = \epsilon \frac{d}{L} + \frac{L-d}{L} \tag{A17}$$

$$\epsilon_x = \frac{(\epsilon-1)^2 d(L-d)}{(\epsilon-1)^2 d(L-d) + \epsilon L^2} \sin^2\phi_0 + \frac{L\epsilon}{\epsilon(L-d)+d} \tag{A18}$$

Note that when $d \to L$, the elements of the dielectric tensor approach the permittivity of region I, i.e. $\epsilon_x, \epsilon_y, \epsilon_z \to \epsilon$ and when $d \to 0$, then $\epsilon_x, \epsilon_y, \epsilon_z \to 1$, as expected. There are two interesting points in (A17) and (A18) that should be

mentioned. The first is that the equivalent permittivities are not functions of frequency (k_0). The second point is that ϵ_y ($= \epsilon_z$) is not a function of incidence angle and variation of ϵ_x with incidence angle is very small. This variation is higher for larger values of ϵ.

A4 Reflection Coefficient of Uniaxial Layered Medium

Consider a multilayer dielectric half-space as shown in Fig. A-19. Suppose each dielectric layer is uniaxial and the optical axes of all the layers are parallel to the x axis. Further assume that a plane wave whose plane of incidence is parallel to the x-y plane is illuminating the stratified medium from above at an angle ϕ_0. The interface of the nth and the $(n+1)$th layers is located at $y = d_n$.

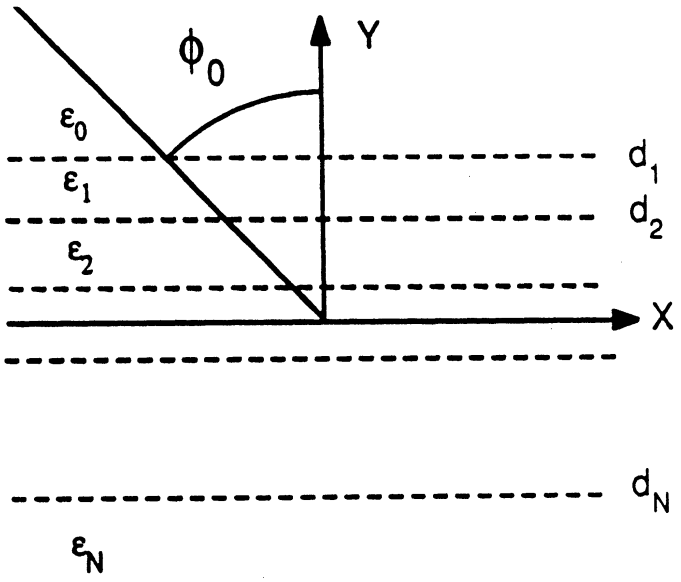

Figure A-19: Plane wave reflection from a stratified uniaxial dielectric half-space.

The dielectric tensor of the nth layer is defined by $\mathbf{D}^n = \epsilon_n \mathbf{E}^n$ and is assumed

to be of the following form

$$\epsilon_n = \epsilon_0 \begin{bmatrix} \epsilon_{xn} & 0 & 0 \\ 0 & \epsilon_n & 0 \\ 0 & 0 & \epsilon_n \end{bmatrix} \tag{A19}$$

and its permeability is that of free space ($\mu_n = \mu_0$). In this situation two plane waves are generated in the dielectric slabs: one ordinary and one extraordinary. For the ordinary wave the electric field and the electric displacement are parallel and both are perpendicular to the principal plane (the plane parallel to the optical axis and the direction of propagation) [Kong, 1985; p. 68], hence the magnetic field is in the x-direction (see Fig. A-19). For the extraordinary wave, however, the electric displacement and the magnetic field lie in the principal plane and the y-z plane respectively which force the electric field to be parallel to the x-axis. Therefore the ordinary or the extraordinary waves can be generated, respectively, by a magnetic or an electric Hertz vector potential having only an x component. For ordinary waves $\mathbf{D}^n = \epsilon_0 \epsilon_n \mathbf{E}^n$ and the magnetic Hertz potential ($\boldsymbol{\Pi}_m^n = \Pi_o^n \hat{x}$) must satisfy the wave equation, i.e.

$$\nabla^2 \Pi_o^n + k_0^2 \epsilon_n \Pi_o^n = 0 \tag{A20}$$

The electric and magnetic fields in terms of the magnetic Hertz potential are given by

$$\mathbf{E}_o^n = ik_0 Y_0 \nabla \times \boldsymbol{\Pi}_m^n \tag{A21}$$

$$\mathbf{H}_o^n = \nabla \times \nabla \times \boldsymbol{\Pi}_m^n \tag{A22}$$

In the case where there is no variation with respect to z (A21) and (A22) reduce to

$$\mathbf{E}_o^n = -ik_0 Z_0 \frac{\partial \Pi_o^n}{\partial y}\hat{z} \tag{A23}$$

$$\mathbf{H}_o^n = -\frac{\partial^2 \Pi_o^n}{\partial y^2}\hat{x} + \frac{\partial^2 \Pi_o^n}{\partial x \partial y}\hat{y} \tag{A24}$$

The electric and magnetic fields associated with the extraordinary wave, as discussed earlier, can be derived from an electric Hertz vector potential, i.e.

$$\mathbf{H}_e^n = -ik_0 Y_0 \nabla \times \boldsymbol{\Pi}_e^n$$

and from Maxwell's equations

$$\nabla \times \mathbf{E}_e^n = k_0^2 \nabla \times \boldsymbol{\Pi}_e^n$$

which implies

$$\mathbf{E}_e^n = k_0^2 \boldsymbol{\Pi}_e^n + \nabla \Phi^n \tag{A25}$$

where Φ^n is an arbitrary scalar function. Using (A19) the electric displacement in the nth layer may be represented by

$$\mathbf{D}_e^n = \epsilon_0[(\epsilon_{xn} - \epsilon_n)E_{ex}^n \hat{x} + \epsilon_n \mathbf{E}_e^n] \tag{A26}$$

Inserting (A25) into (A26) and noting that

$$\mathbf{D}_e^n = \nabla\nabla \cdot \boldsymbol{\Pi}_e^n - \nabla^2 \boldsymbol{\Pi}_e^n$$

we get

$$\nabla^2 \boldsymbol{\Pi}_e^n + \epsilon_{xn} k_0^2 \boldsymbol{\Pi}_e^n + (\epsilon_{xn} - \epsilon_n) \frac{\partial \Phi^n}{\partial x} \hat{x} + \nabla \left(\epsilon_n \Phi^n - \nabla \cdot \boldsymbol{\Pi}_e^n \right) = 0 \qquad \text{(A27)}$$

So far no condition has been imposed on the scalar function Φ^n. To simplify the differential equation (A27) let $\nabla \cdot \boldsymbol{\Pi}_e^n = \epsilon_n \Phi^n$ be the gauge condition. Therefore the electric Hertz vector potential must satisfy

$$\nabla^2 \Pi_e^n + \epsilon_{xn} k_0^2 \Pi_e^n + \frac{\epsilon_{xn} - \epsilon_n}{\epsilon_n} \frac{\partial^2 \Pi_e^n}{\partial x^2} = 0 \qquad \text{(A28)}$$

In the special case where $\partial/\partial z = 0$ the magnetic and electric fields of the extraordinary waves can be obtained from

$$\mathbf{H}_e^n = i k_0 Z_0 \frac{\partial \Pi_e^n}{\partial y} \hat{z} \qquad \text{(A29)}$$

$$\mathbf{E}_e^n = (k_0^2 \Pi_e^n + \frac{1}{\epsilon_n} \frac{\partial^2 \Pi_e^n}{\partial x^2}) \hat{x} + \frac{1}{\epsilon_n} \frac{\partial^2 \Pi_e^n}{\partial x \partial y} \hat{y} \qquad \text{(A30)}$$

The solution of the differential equations (A20) and (A28) subject to plane wave incidence can be represented by $e^{i(k_{ox}^n x \pm k_{oy}^n y)}$ and $e^{i(k_{ex}^n x \pm k_{ey}^n y)}$ respectively and upon substitution of these solutions in the corresponding differential equations the following dispersion relationships are obtained

$$(k_{ox}^n)^2 + (k_{oy}^n)^2 = \epsilon_n k_0^2 \qquad \text{(A31)}$$

$$\frac{1}{\epsilon_n} (k_{ex}^n)^2 + \frac{1}{\epsilon_{xn}} (k_{ey}^n)^2 = k_0^2 \qquad \text{(A32)}$$

Imposing the phase matching condition, i.e. $k_{ox}^n = k_{ex}^n = k_0 \sin \phi_0$, the dispersion relations simplify to

$$k_{oy}^n = k_0 \sqrt{\epsilon_n - \sin \phi_0}$$

$$k_{ey}^n = k_0 \sqrt{\frac{\epsilon_{xn}}{\epsilon_n}} \sqrt{\epsilon_n - \sin^2 \phi_0}$$

The Hertz vector potentials in the nth layer can be written as

$$\Pi_o^n = \left[A_i^n e^{-ik_{oy}^n y} + A_r^n e^{ik_{oy}^n y} \right] e^{ik_0 \sin\phi_0 x} \tag{A33}$$

$$\Pi_e^n = \left[B_i^n e^{-ik_{ey}^n y} + B_r^n e^{ik_{ey}^n y} \right] e^{ik_0 \sin\phi_0 x} \tag{A34}$$

In (A33)-(A34) the subscripts i and r in the coefficients denote the propagation in the negative and positive y direction respectively.

Since there is no variation with respect to z, the incident wave can be decomposed into parallel (H) and perpendicular (E) polarization which would excite extraordinary and ordinary waves respectively. For E polarization the electric and magnetic fields in each region can be obtained from (A23) and (A24) using (A33). In region 0, A_i^0 is proportional to the incident amplitude, and $-A_r^0/A_i^0 = R_E$ is the total reflection coefficient. In region $N+1$, which is semi-infinite, $A_r^{N+1} = 0$. Imposing the boundary conditions, which requires continuity of tangential electric and magnetic fields at each dielectric interface, we can relate the field amplitudes in the nth region to those of $(n+1)$th region. After some algebraic manipulation, the following recursive relationship can be obtained

$$-\frac{A_r^n}{A_i^n} = \frac{(-A_r^{n+1}/A_i^{n+1}) + \Gamma_o^n e^{-i2k_{oy}^{n+1} d_{n+1}}}{(-A_r^{n+1}/A_i^{n+1})\Gamma_o^n + e^{-i2k_{oy}^{n+1} d_{n+1}}} e^{-i2k_{oy}^n d_{n+1}} \tag{A35}$$

where

$$\Gamma_o^n = \frac{\sqrt{\epsilon_n - \sin^2\phi} - \sqrt{\epsilon_{n+1} - \sin^2\phi}}{\sqrt{\epsilon_n - \sin^2\phi} + \sqrt{\epsilon_{n+1} - \sin^2\phi}}$$

Starting from $-A_r^{N+1}/A_i^{N+1} = 0$ and using (A35) repeatedly R_E can be found.

For H polarization incidence the extraordinary waves are excited and using (A34) in (A29) and (A30) the electric and magnetic fields in each region can be obtained. Following a similar procedure outlined for the E polarization case an identical recursive formula as given by (A35) can be derived. The only difference is that A is replaced by B, k_{oy} by k_{ey} and Γ_o^n becomes Γ_e^n which is given by

$$\Gamma_e^n = \frac{\sqrt{\epsilon_{x(n+1)}\epsilon_{n+1}}\sqrt{\epsilon_n - \sin^2\phi} - \sqrt{\epsilon_{xn}\epsilon_n}\sqrt{\epsilon_{n+1} - \sin^2\phi}}{\sqrt{\epsilon_{x(n+1)}\epsilon_{n+1}}\sqrt{\epsilon_n - \sin^2\phi} + \sqrt{\epsilon_{xn}\epsilon_n}\sqrt{\epsilon_{n+1} - \sin^2\phi}}$$

A5 Numerical Examples

As mentioned earlier (A10) and (A15) can be solved using numerical methods. Here we use Newton's method to find the zeroes of the functions given by (A10) and (A15) in which k_x^I is expressed in terms of k_x^{II} using (A11). Before searching for zeroes we note that these functions are odd functions of k_x^{II}, that is, if κ is a solution so would be $-\kappa$ and both would give identical solutions for the equivalent permittivity as given by (A14).

To study the behavior of the equivalent dielectric tensor elements, we consider a medium with $\epsilon = 4 + i1$ and $L = \lambda_0/4$. Figure A-3 and A-4 depict the variation of the real and imaginary parts of ϵ_x (H polarization) and $\epsilon_y = \epsilon_z$ (E polarization) versus angle of incidence for $d/L = 0.5$. It is shown that the dependency with the incidence angle is very small and these results are in agreement with (A17) and (A18) within 10%. The real and imaginary parts of the equivalent permittivities as a function of d/L for incidence angle $\phi_0 = 45°$ are shown in Figs. A-5 and A-6

respectively.

As L/λ_0 increases the propagation loss factors ($\mathrm{Im}[k_y]$) of different modes become comparable to each other. For example, if $L/\lambda_0 = m/2$, where m is an integer, there would be at least two modes with equal propagation loss factor. Figures A-7a through A-7d show the location of zeroes of (A10) in k_x^{II}-plane for $d/L = 0.5$, $\phi_0 = 45°$, and four values of L/λ_0. The real and imaginary parts of the equivalent permittivities as a function of L/λ_0 for $d/L = 0.5$ and $\phi_0 = 45°$ are shown in Figs. A-8 and A-9. The discontinuity in the equivalent permittivities at integer multiples of $\lambda_0/2$ are due to the abrupt changes in the location of the zeroes in the k_x^{II}-plane which correspond to the dominant modes.

To check the validity and applicability of this technique we compare the reflection coefficient of a corrugated surface using the moment method as discussed in Section 2.4 with the reflection coefficient of the equivalent anisotropic medium as derived in Section A4. The geometry of the scattering problem is depicted in Fig. 7. We consider a case where $L = \lambda_0/4$, $d = t = \lambda_0/8$, $\epsilon_1 = 4 + i1$, and $\epsilon_2 = 15 + i7$. The tensor elements for these parameters are found to be $\epsilon_x = 1.81 + i0.15$, $\epsilon_y = \epsilon_z = 2.6 + i0.58$. Figures A-10 and A-11, respectively, compare the amplitude and phase of the reflection coefficients for both E and H polarizations. Excellent agreement between the results based on the moment method and the equivalent layer is an indication for the validity of the model. As frequency increases, because of presence of higher order modes, the discrepancy between the moment method and the equivalent layer results becomes more evi-

dent. Figures A-12 and A-13 show the reflection coefficient of a corrugated layer with $L/\lambda_0 = 0.4$, $d = t = 0.2\lambda$, $\epsilon_1 = 4 + i1$, and $\epsilon_2 = 15 + i7$. In this case $\epsilon_x = 1.81 + i0.2$, $\epsilon_y = \epsilon_z = 2.77 + i0.78$ and the agreement is still very good, but for $L > \lambda_0/2$ where more than one Bragg mode exists the model fails to predict the reflection coefficient accurately.

Success of the equivalent layer in modeling rectangular corrugations can be extended to arbitrary periodic geometries. By approximating the cross section of the periodic surface with staggered increments of equal height, the surface can be viewed as a stack of corrugated layers (see Fig. A-14). The height of each layer ΔH must be chosen such that $\Delta H \leq \lambda/10$ where λ is the wavelength in the material. Then each corrugated layer can be modeled by an equivalent anisotropic slab and the reflection coefficient of the resultant uniaxial layered medium can be obtained. To demonstrate this method consider a wedge-shape microwave absorber with permittivity $\epsilon = 2+i0.5$, period $L = 0.4\lambda_0$, wedge height $H = 1.5\lambda_0$, and base height $D = 1\lambda_0$. The number of layers considered here is 30 and the corresponding reflection coefficients for both E and H polarizations as a function of incidence angle is depicted in Fig. A-15.

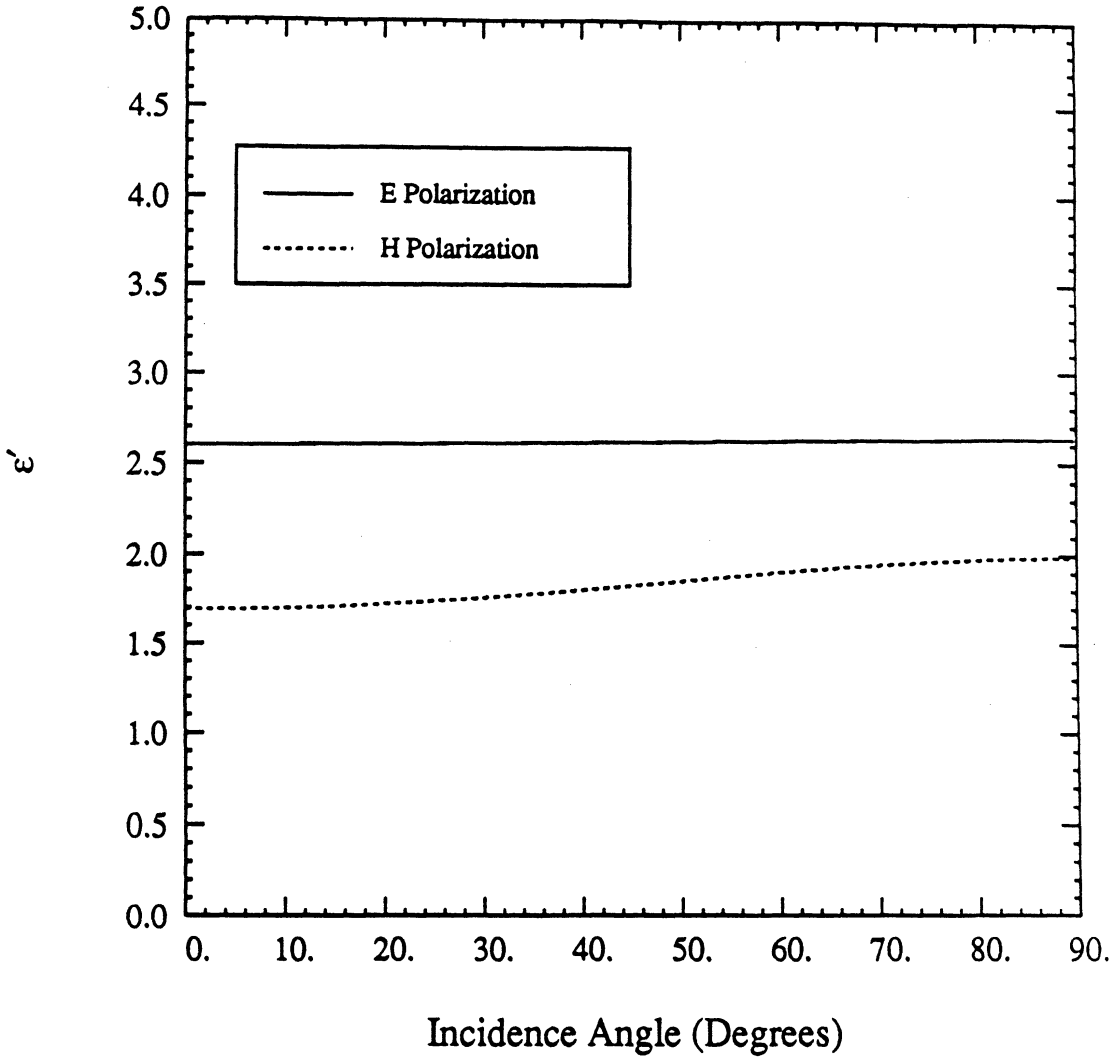

Figure A-3: Real part of the equivalent dielectric tensor elements for periodic slab medium with $L = \lambda_0/4$, $\epsilon = 4 + i1$, and $d/L = 0.5$ versus incidence angle; ϵ_x (H polarization), $\epsilon_y = \epsilon_z$ (E polarization).

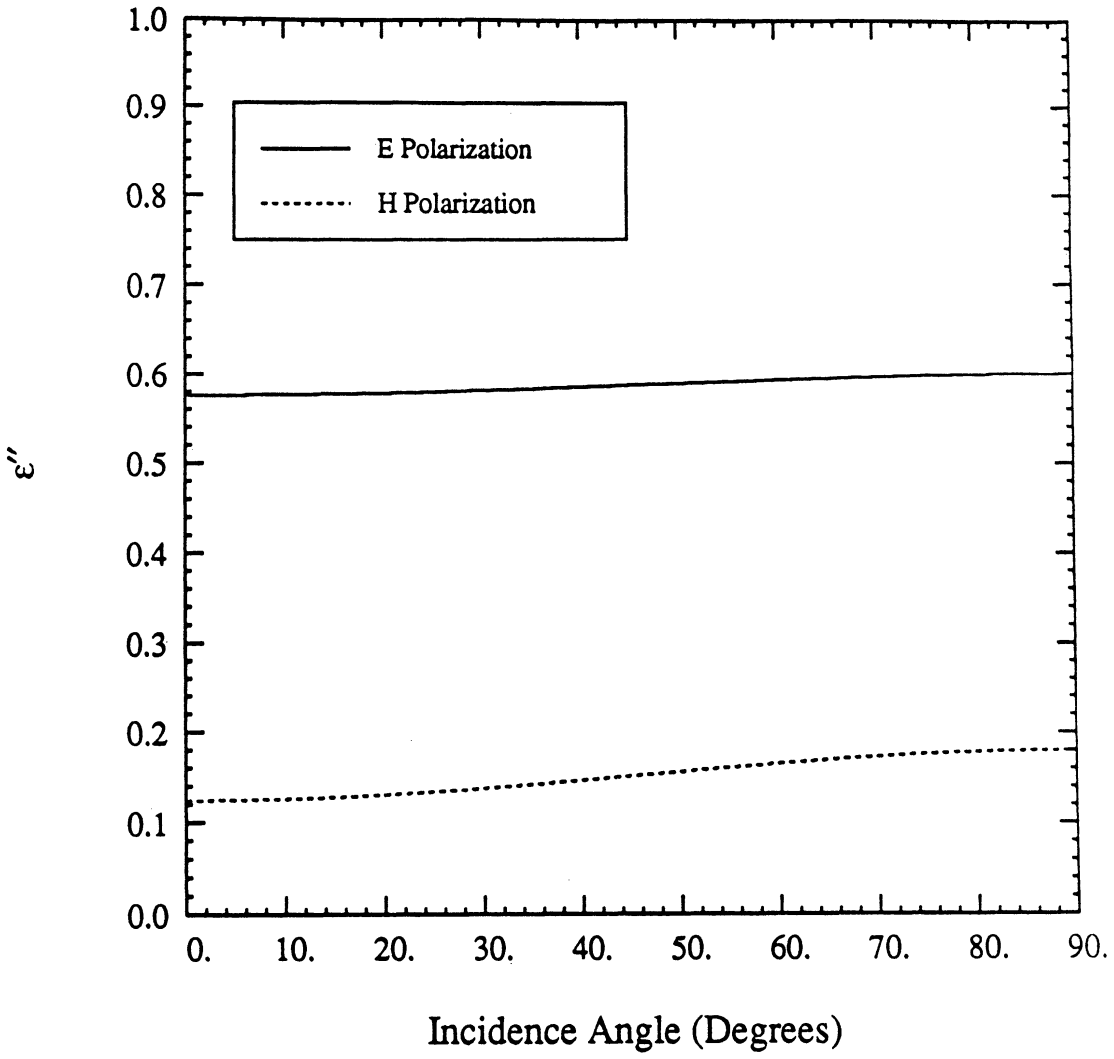

Figure A-4: Imaginary part of the equivalent dielectric tensor elements for periodic slab medium with $L = \lambda_0/4$, $\epsilon = 4 + i1$, and $d/L = 0.5$ versus incidence angle; ϵ_x (H polarization), $\epsilon_y = \epsilon_z$ (E polarization).

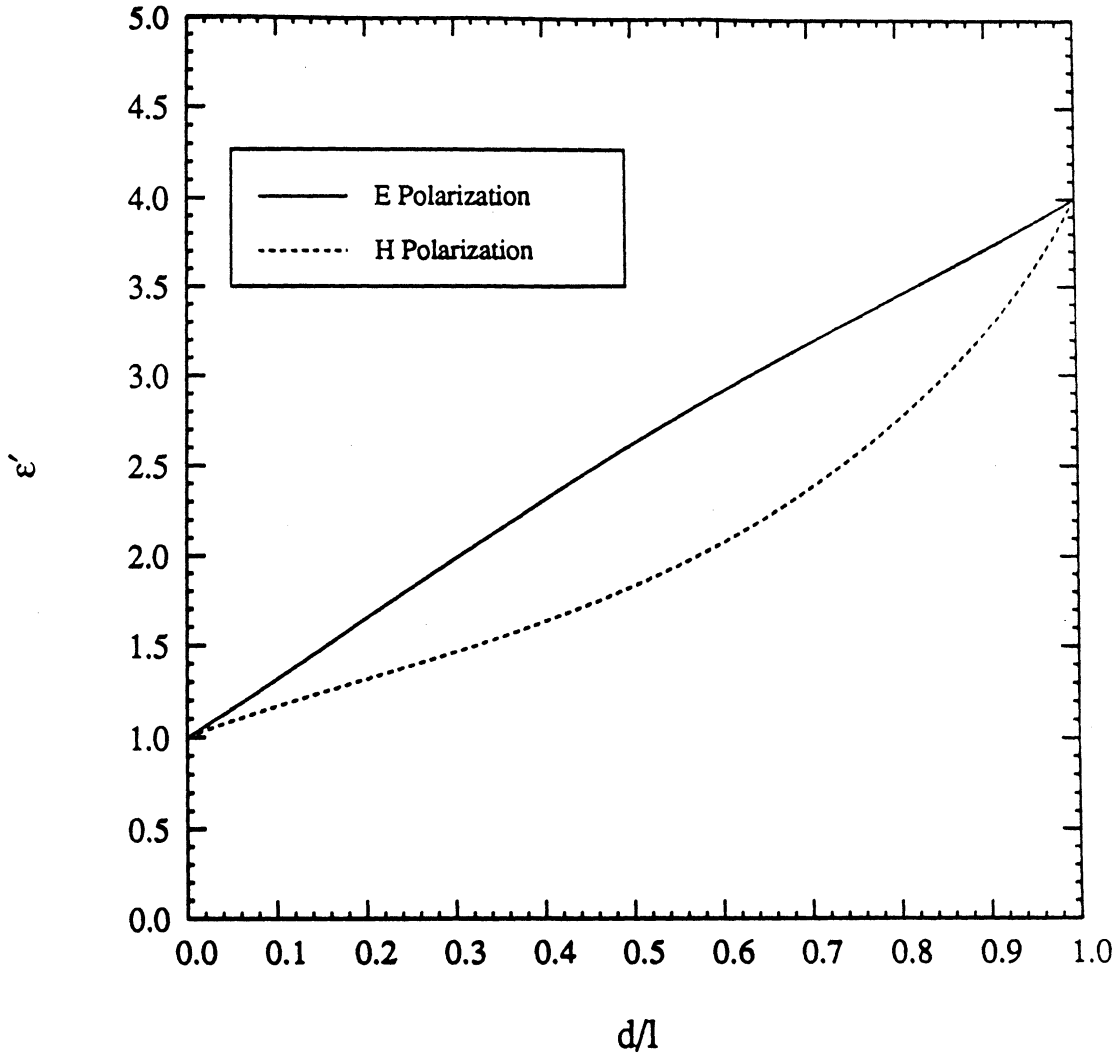

Figure A-5: Real part of the equivalent dielectric tensor elements for a periodic slab medium with $L = \lambda_0/4$, $\epsilon = 4 + i1$, and $\phi_0 = 45°$ versus d/L; ϵ_x (H polarization), $\epsilon_y = \epsilon_z$ (E polarization).

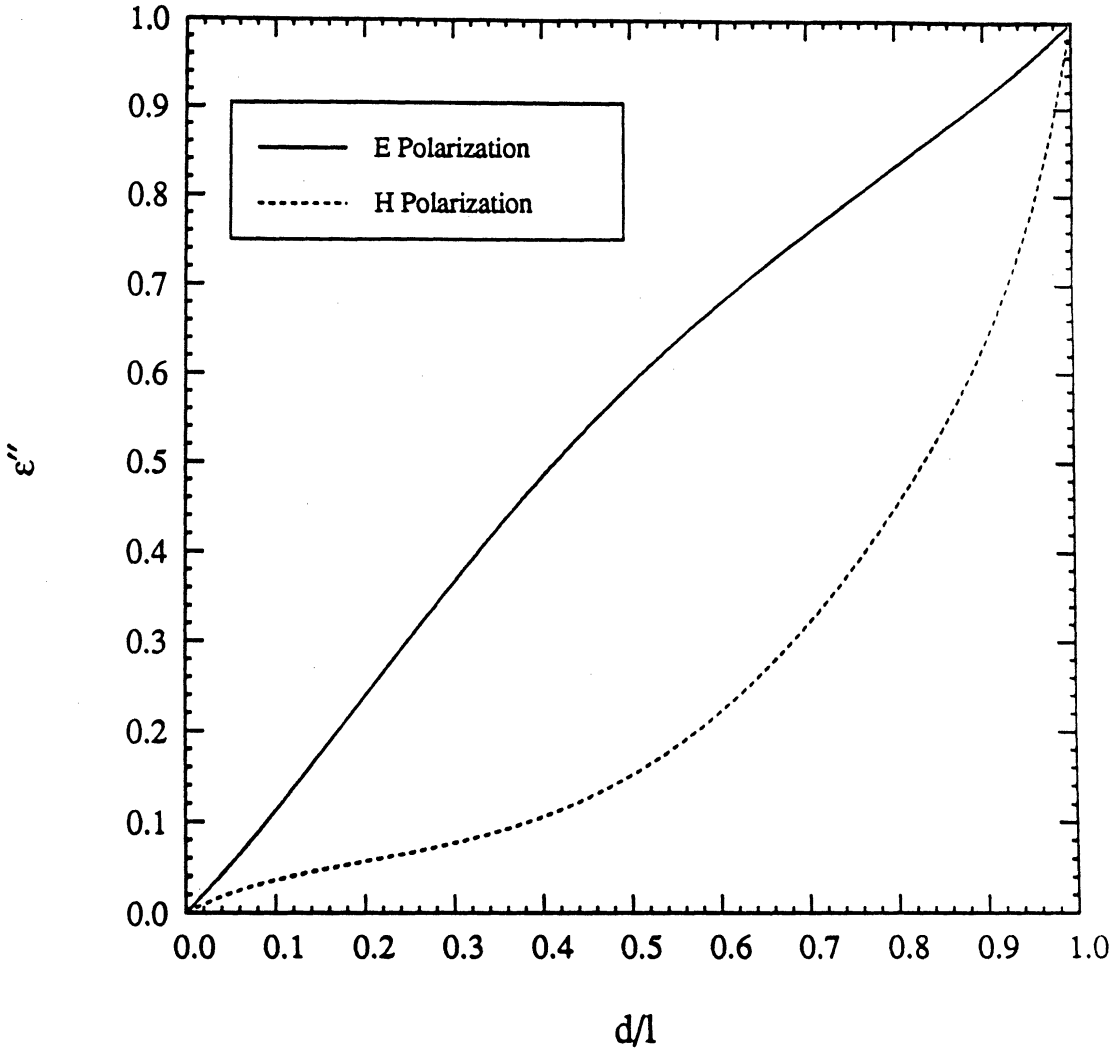

Figure A-6: Imaginary part of the equivalent dielectric tensor elements for periodic slab medium with $L = \lambda_0/4$, $\epsilon = 4 + i1$, and $\phi_0 = 45°$ versus d/L; ϵ_x (H polarization), $\epsilon_y = \epsilon_z$ (E polarization).

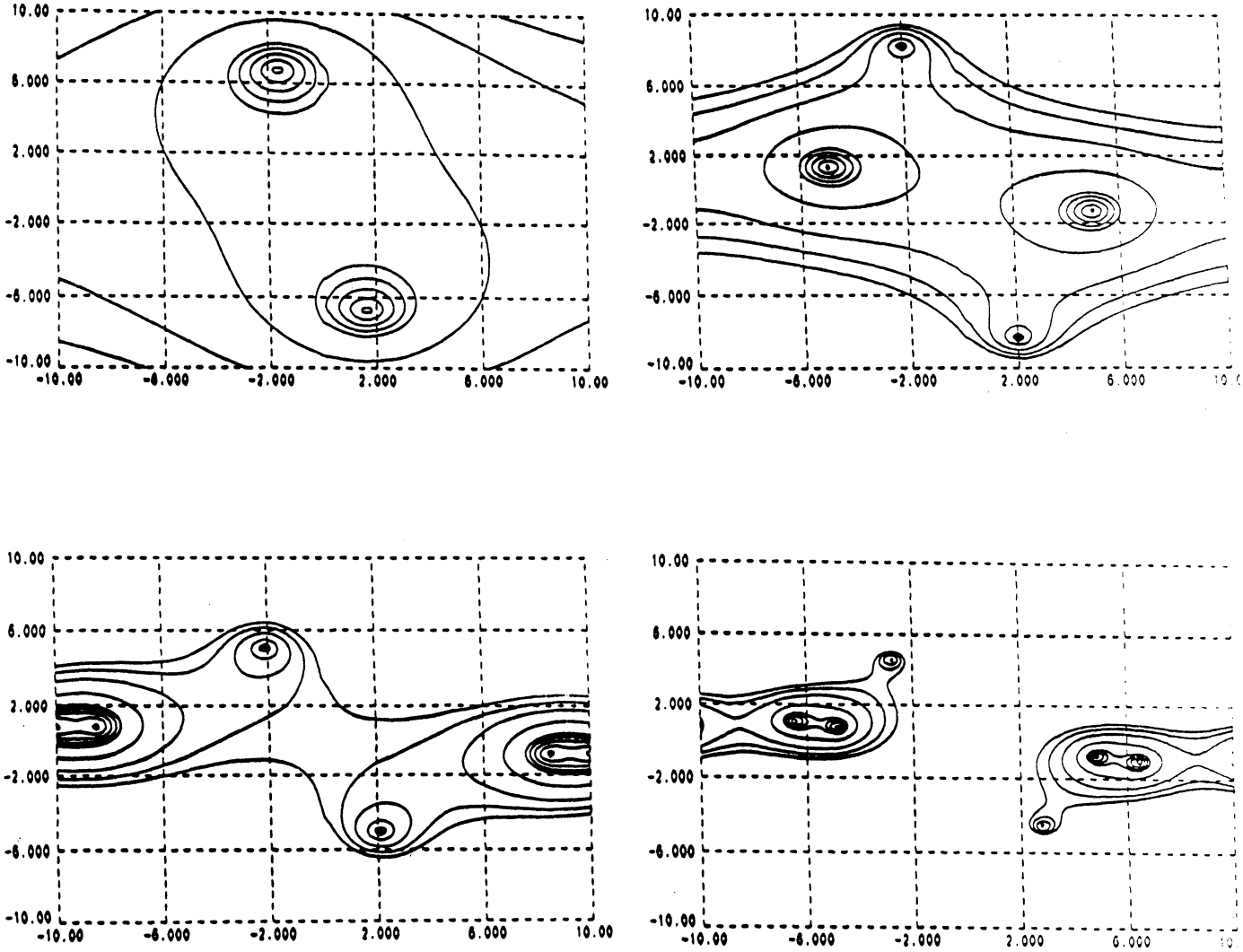

Figure A-7: Location of zeros of (A-10)in the k_x^{II}-plane for for the periodic slab medium with $\epsilon = 4 + i1$, $\phi_0 = 45°$, $d/L = 0.5$, and (a) $L = 0.2\lambda_0$, (b) $L = 0.5\lambda_0$, (c) $L = 0.8\lambda_0$, (d) $L = 1.4\lambda_0$.

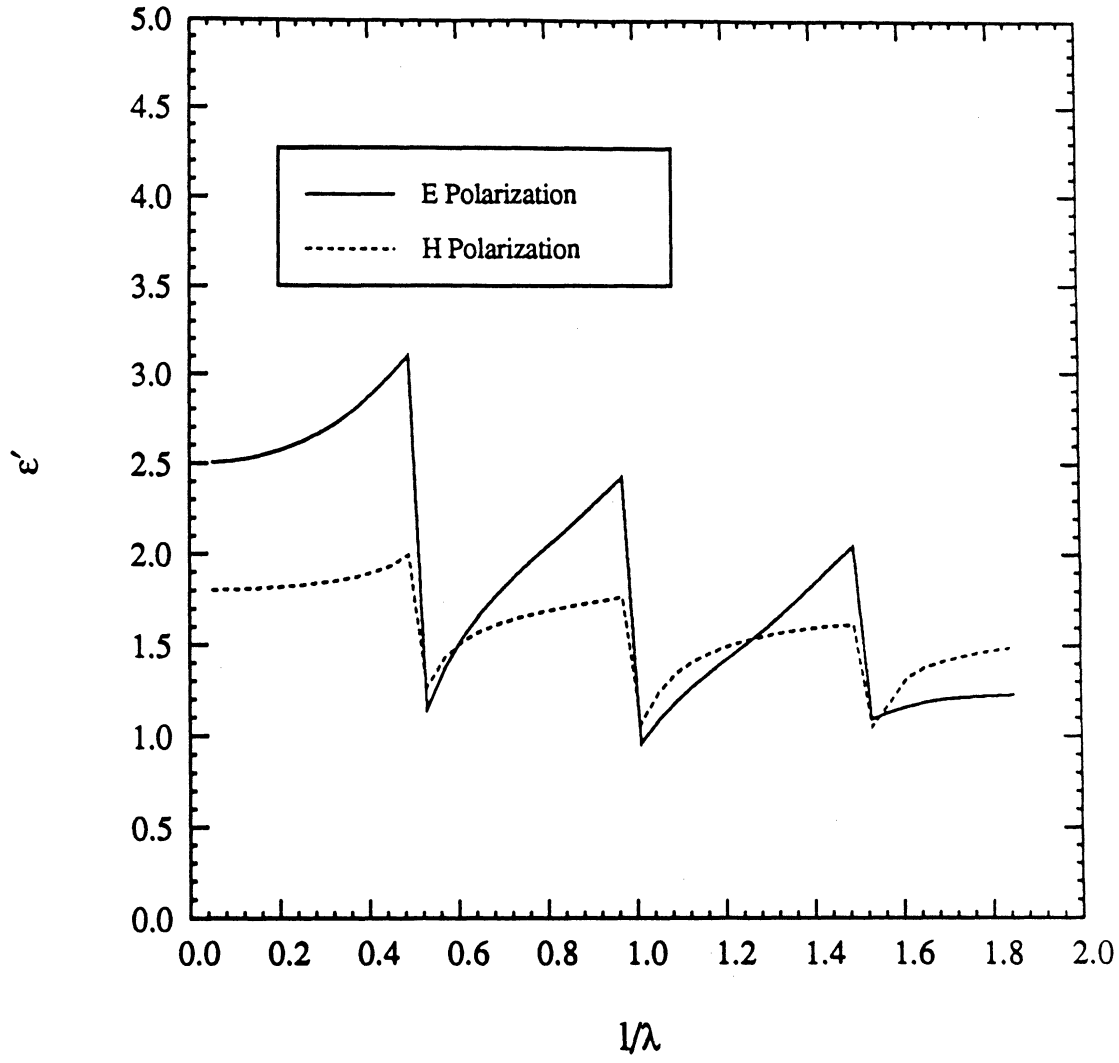

Figure A-8: Real part of the equivalent dielectric tensor elements for periodic slab medium with $\epsilon = 4 + i1$, and $\phi_0 = 45°$, and $d/L = 0,5$ versus L/λ_0; ϵ_x (H polarization), $\epsilon_y = \epsilon_z$ (E polarization).

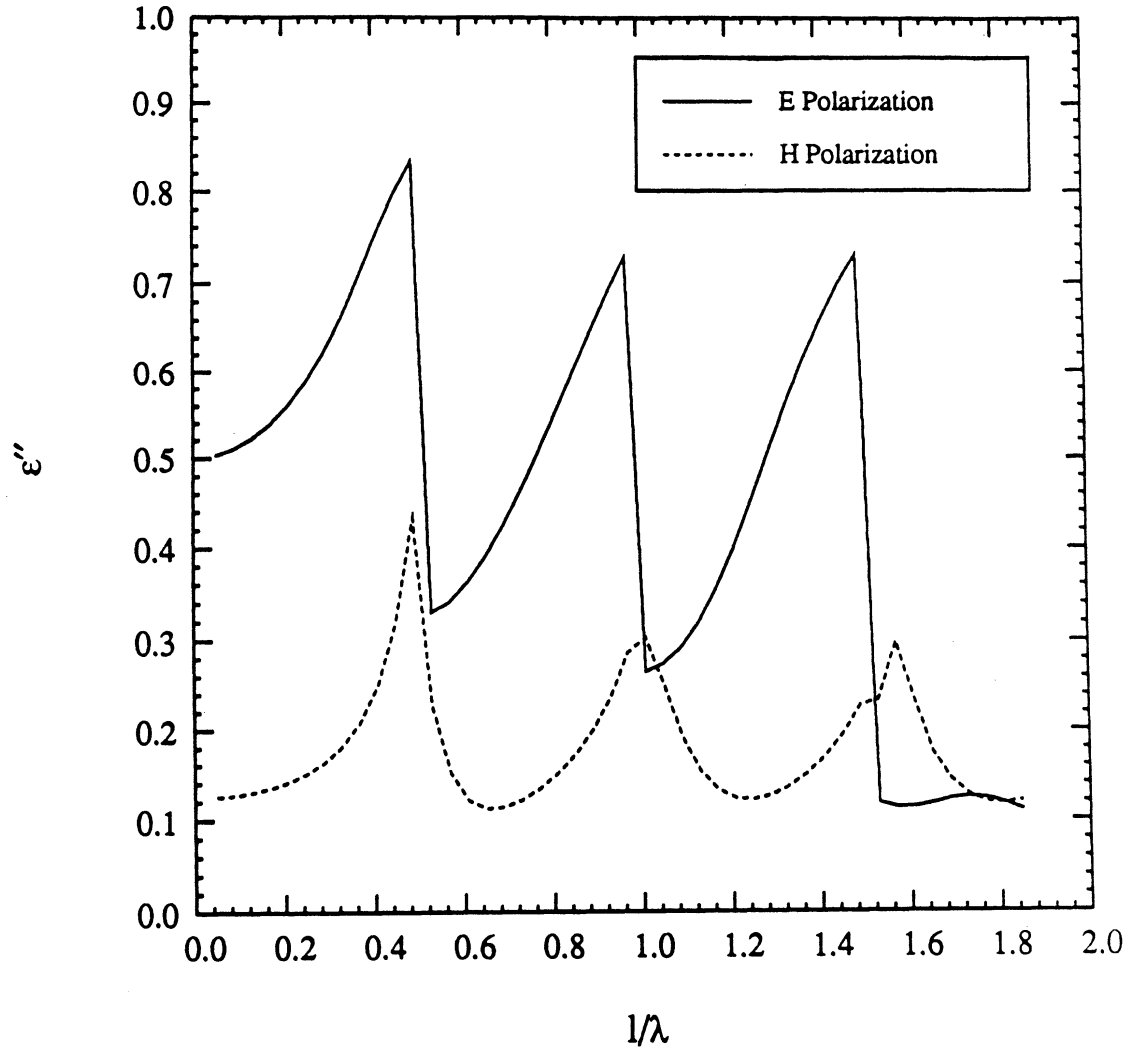

Figure A-9: Imaginary part of the equivalent dielectric tensor elements for periodic slab medium with $\epsilon = 4 + i1$, and $\phi_0 = 45°$, and $d/L = 0,5$ versus L/λ_0; ϵ_x (H polarization), $\epsilon_y = \epsilon_z$ (E polarization).

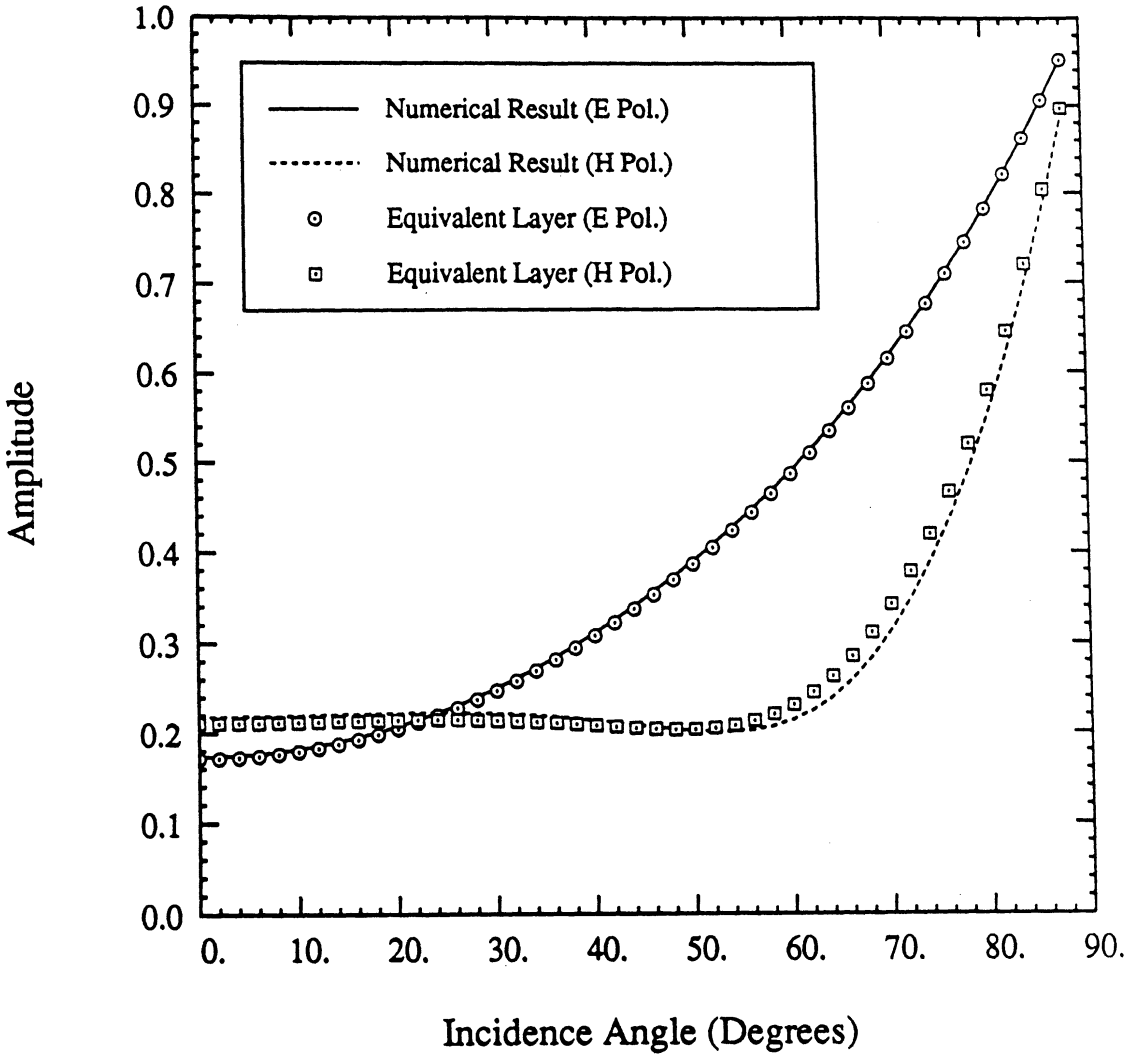

Figure A-10: Amplitude of reflection coefficient of a corrugated surface for both E and H polarizations versus incidence angle; $L = 0.25\lambda_0$.

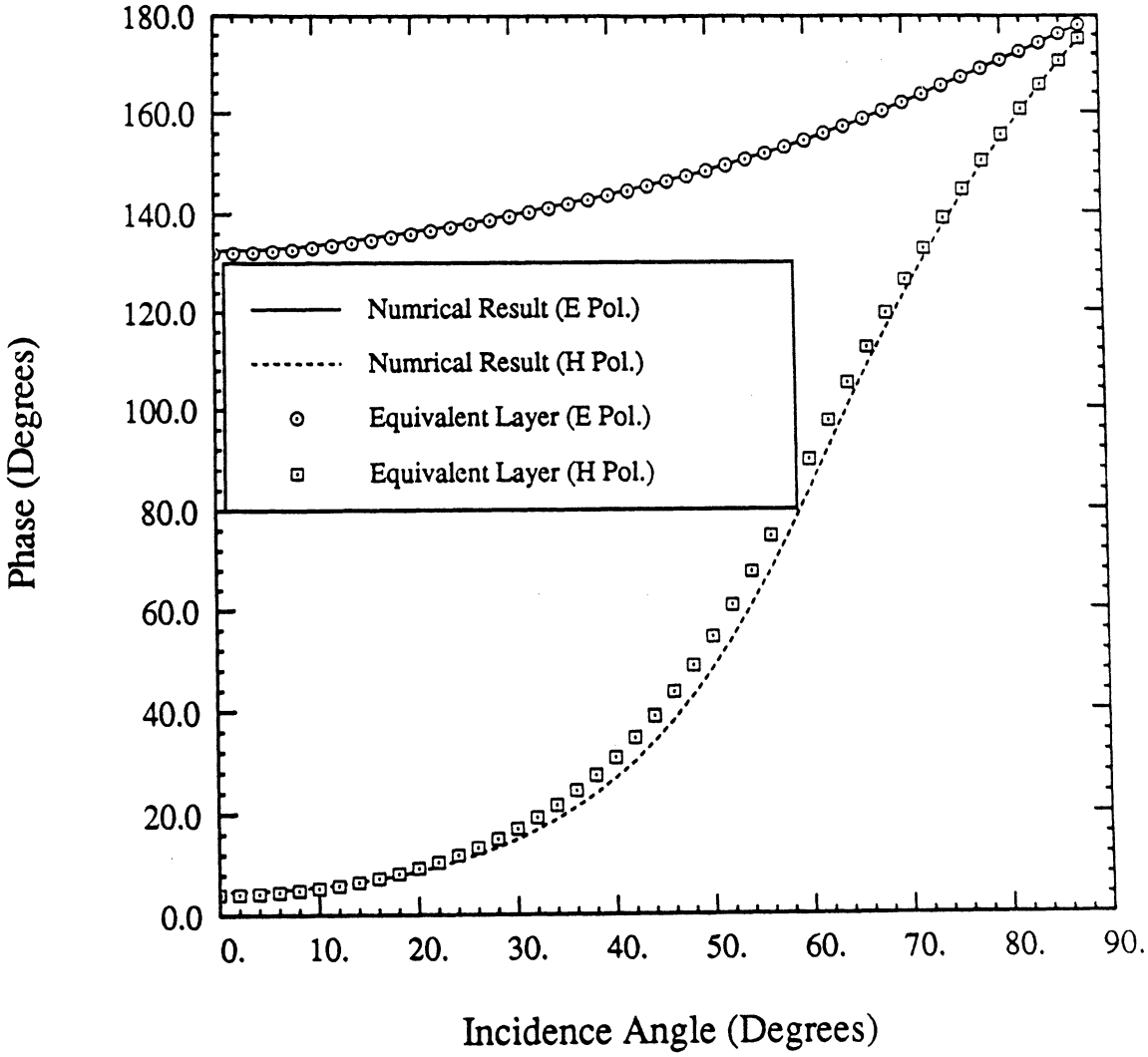

Figure A-11: Phase of reflection coefficient of a corrugated surface for both E and H polarizations versus incidence angle; $L = 0.25\lambda_0$.

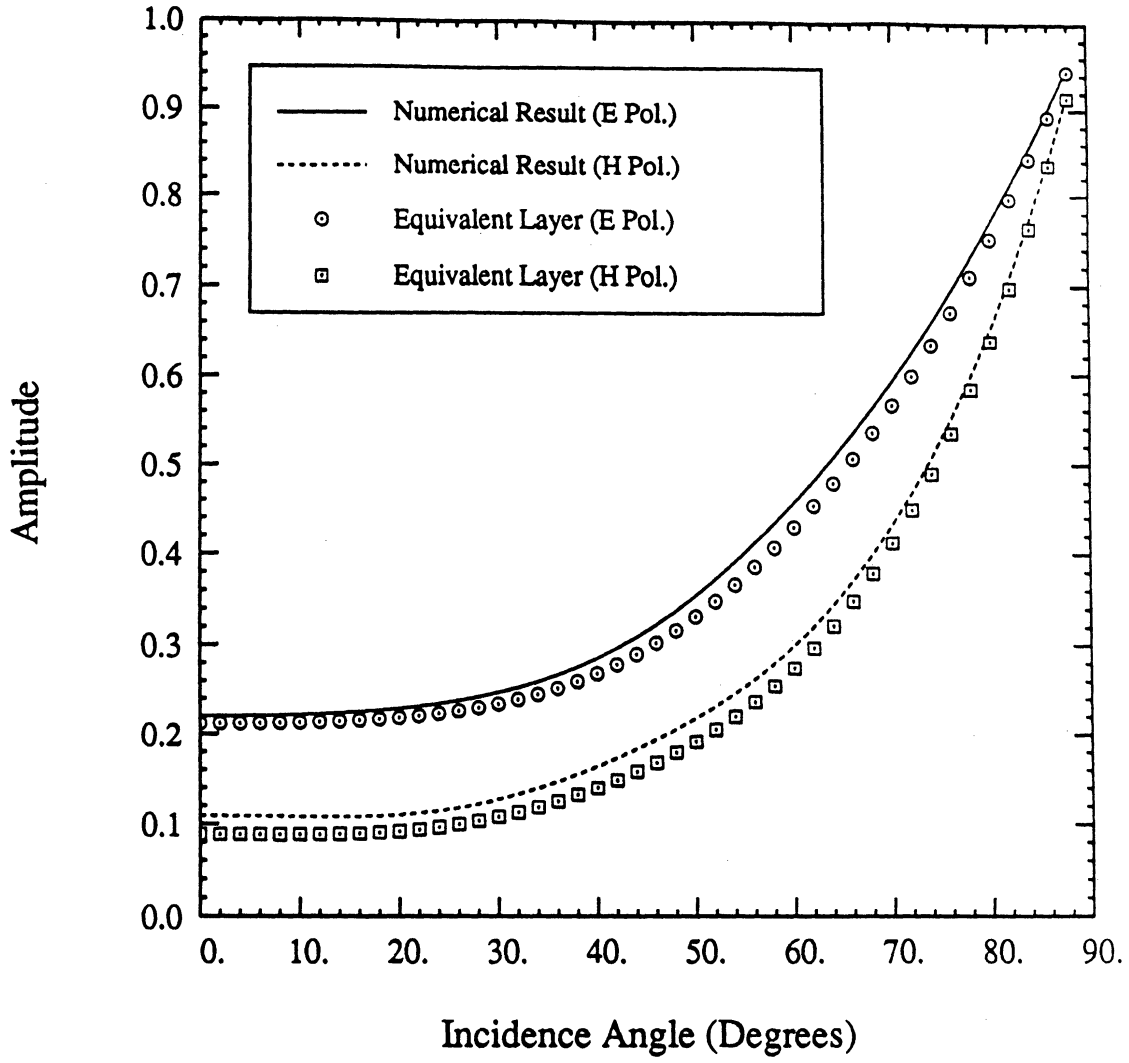

Figure A-12: Amplitude of reflection coefficient of a corrugated surface for both E and H polarizations versus incidence angle; $L = 0.4\lambda_0$.

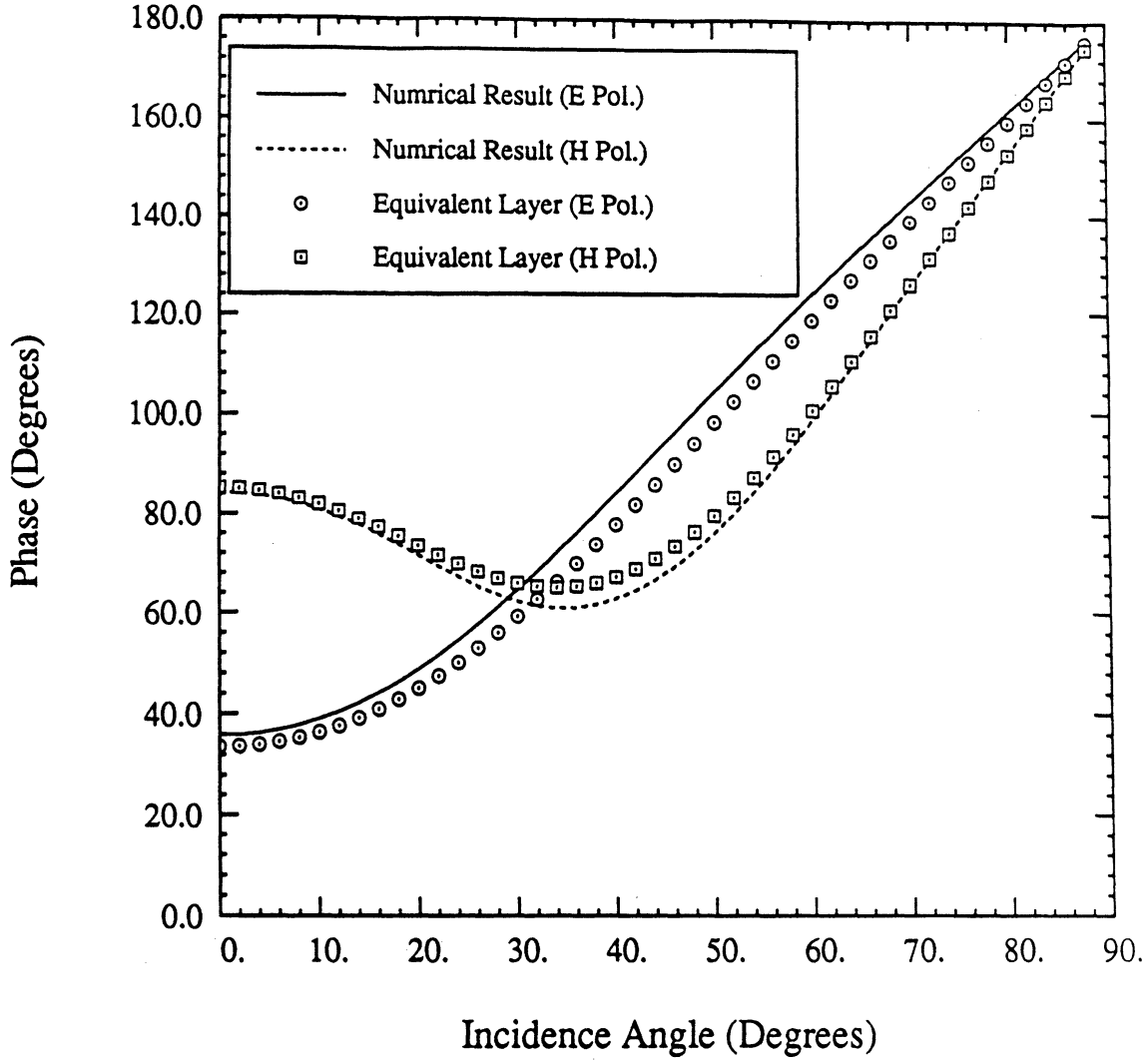

Figure A-13: Phase of reflection coefficient of a corrugated surface for both E and H polarizations versus incidence angle; $L = 0.4\lambda_0$.

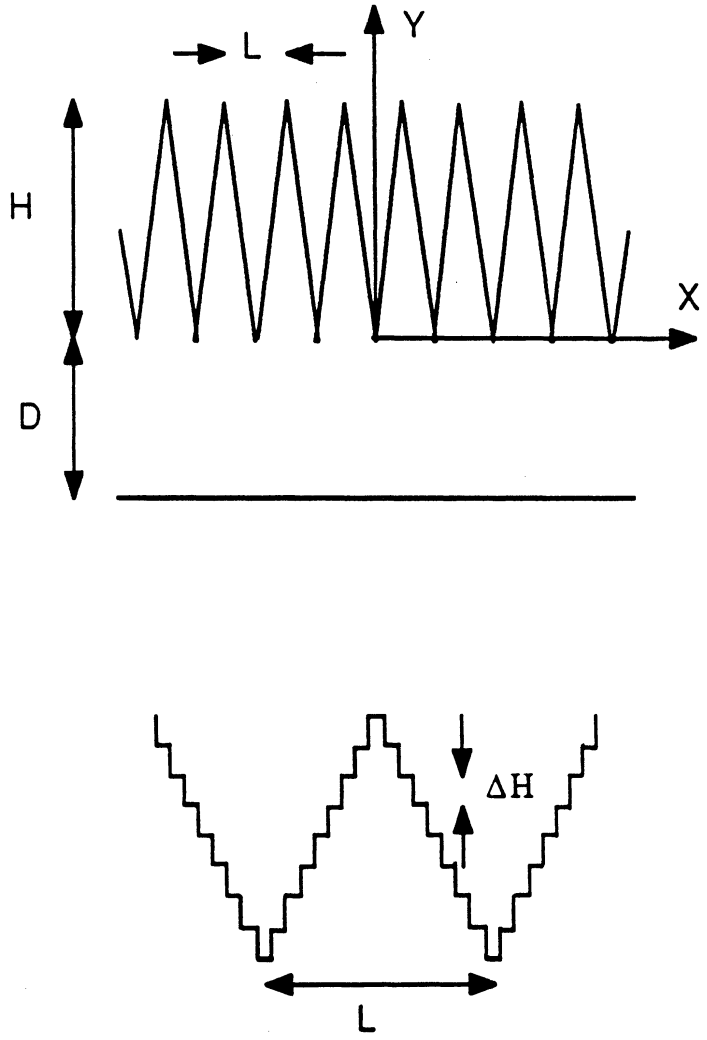

Figure A-14: Geometry of a wedge-shape microwave absorber and its staircase approximation.

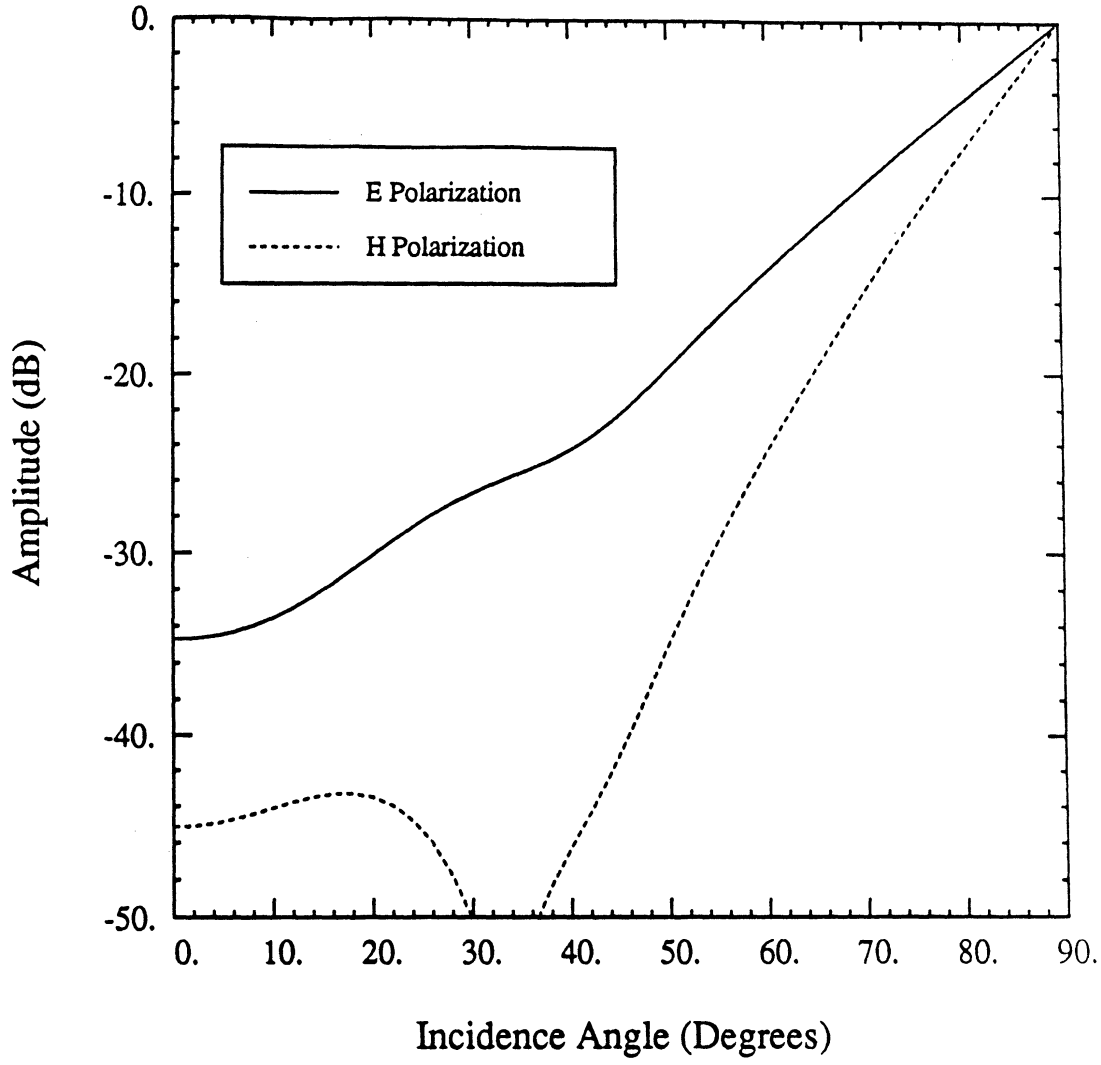

Figure A-15: Amplitude of reflection coefficient of a wedge-shape microwave absorber for both E and H polarizations versus incidence angle; $L = 0.4\lambda_0$, $H = 1.5\lambda_0$, $D = 1\lambda_0$, and $\epsilon = 2.5 + i0.5$.